

# Modelling the Dynamics of Global Monopoles

Inyong Cho\* and Jemal Guven<sup>† ‡</sup>

*Institute of Cosmology, Department of Physics and Astronomy,*

*Tufts University, Medford, Massachusetts 02155, USA*

(October 17, 2018)

## Abstract

A thin wall approximation is exploited to describe a global monopole coupled to gravity. The core is modelled by de Sitter space; its boundary by a thin wall with a constant energy density; its exterior by the asymptotic Schwarzschild solution with negative gravitational mass  $M$  and solid angle deficit,  $\Delta\Omega/4\pi = 8\pi G\eta^2$ , where  $\eta$  is the symmetry breaking scale. The deficit angle equals  $4\pi$  when  $\eta = 1/\sqrt{8\pi G} \equiv M_p$ . We find that: (1) if  $\eta < M_p$ , there exists a unique globally static non-singular solution with a well defined mass,  $M_0 < 0$ .  $M_0$  provides a lower bound on  $M$ . If  $M_0 < M < 0$ , the solution oscillates. There are no inflating solutions in this symmetry breaking regime. (2) if  $\eta \geq M_p$ , non-singular solutions with an inflating core and an asymptotically cosmological exterior will exist for all  $M < 0$ . (3) if  $\eta$  is not too large, there exists a finite range of values of  $M$  where a non-inflating monopole will also exist. These solutions appear to be metastable towards inflation. If  $M$  is positive all solutions are singular. We provide a detailed description of the

---

\*Electronic address: cho@cosmos2.phy.tufts.edu

<sup>†</sup>Electronic address: jemal@nuclecu.unam.mx

<sup>‡</sup>Permanent Address: Instituto de Ciencias Nucleares, Universidad Nacional Autónoma de México.

Apdo. Postal 70-543, 04510 México, D.F., MEXICO

configuration space of the model for each point in the space of parameters,  $(\eta, M)$  and trace the wall trajectories on both the interior and the exterior spacetimes. Our results support the proposal that topological defects can undergo inflation.

## I. INTRODUCTION

Phase transitions occurring in the early universe can give rise to topological defects of various kinds; these may be domain walls, strings and monopoles as well as more exotic objects [1]. Recently Vilenkin [2] and Linde [3] proposed that topological defects could inflate when the symmetry breaking scale,  $\eta \gtrsim \mathcal{O}(m_p)$ , thereby providing natural seeds for an inflating universe. This was recently confirmed numerically by Sakai *et al.* [4] who showed that domain walls and global monopoles will inflate if  $\eta \gtrsim 0.33m_p$ . However, until now, there has been no analytical confirmation of their results.

The simplest defects are global monopoles which are localized in all three spatial directions. Barriola and Vilenkin [5] obtained the simplest static global monopole solution coupled to gravity. Asymptotically, the spacetime is described by the static line element,

$$ds^2 = -A_M dT_M^2 + A_M^{-1} dR^2 + R^2 d\Omega^2, \quad (1.1)$$

where

$$A_M = 1 - 8\pi G\eta^2 - \frac{2GM}{R}. \quad (1.2)$$

The gravitational mass is given by the parameter,  $M$ . There are several features of this asymptotic spacetime which are unusual:

At infinity, this spacetime is not flat. There is a solid angle deficit,  $\Delta/4\pi \simeq 8\pi G\eta^2$ , determined completely by the symmetry breaking scale,  $\eta$ . The occurrence of a deficit angle is a consequence of the non-trivial topology of the field configuration outside the monopole: non-vanishing gradients along non-radial directions give an energy density outside which

falls off slowly,  $\sim \eta^2/R^2$ . Eq. (1.1) is then the most general spherically symmetric solution of the Einstein equations consistent with such a source. This is analogous to a global string [6].

As Harari and Lousto pointed out, the mass parameter in this static metric is always negative [7]. This is not, however, a violation of the positive mass theorem — the spacetime is not asymptotically flat so that the gravitational mass does not coincide with the ADM mass at infinity [8].

A consequence of the slow falloff is that the total energy of the monopole diverges linearly. To regularize this energy we need to introduce a cutoff at some large radius,  $R^*$ . This cutoff will be provided by the correlation length of the scalar field,  $\xi$ . In cosmology, an upper bound on  $\xi$  is provided by the horizon size.

When the solid angle deficit exceeds  $4\pi$ , ( $8\pi G\eta^2 > 1$ ), the roles of  $R$  and  $T_M$  get interchanged. The exterior solution which corresponds to Barriola and Vilenkin's ansatz is no longer static. This is precisely the regime where topological inflation is predicted to occur and is the regime we will be particularly interested in.

In this paper, we present a model of a global monopole which is tractable analytically and, we believe, includes all of its essential features. The core of the global monopole is approximated by a spherically symmetric region of false vacuum, with energy density  $\rho$ , and radius  $r$ . Outside this core is described by a spherically symmetric region with energy density  $\eta^2/R^2$  and thus described by the asymptotic static metric (1.1).

If the approximation stops here, a static equilibrium exists between these two spacetime geometries only when

$$r = \frac{\eta}{\sqrt{\rho}}, \quad (1.3)$$

and the mass assumes the negative value,

$$M = -\frac{8\pi}{3} \frac{\eta^3}{\sqrt{\rho}}. \quad (1.4)$$

For a given theory this solution is unique. However, the model suffers from the shortcoming that it only describes a static equilibrium and predicts such an equilibrium for all values of  $\eta$ ;

it does not possess the scope to describe non-static configurations. This is essentially because the energy density of false vacuum is constant. In general, when false vacuum is converted to true vacuum (with constant solid angle deficit), the energy released is transferred to the core boundary [9]. This boundary plays an essential dynamical role. The necessary refinement of the model is to introduce a surface layer with energy density,  $\sigma$ , on the core boundary. On dimensional grounds, we expect  $\rho \sim \eta^4$  and  $\sigma \sim \eta^3$ . The Einstein equations now determine the motion of  $r$ .

If  $\eta < M_p$ <sup>1</sup>, we find stable oscillating solutions for each negative value of  $M$  above some threshold. These solutions are the analogues of Harari and Lousto's static approximation.

If  $\eta \geq M_p$ , non-singular solutions with inflating cores and asymptotically cosmological exteriors exist for all  $M < 0$ . There exists some critical value of  $\eta$ ,  $\eta_c > M_p$  above which all monopoles inflate.

For each  $\eta$  in the interval,  $M_p < \eta < \eta_c$  a stable oscillating monopole will co-exist with an inflating one of the same mass in some strictly negative band of values of  $M$ .

These solutions have the virtue that they are non-singular everywhere.

If  $M > 0$ , all solutions collapse to form a black hole. There also exist collapsing monopole solutions with  $M < 0$  which terminate in a naked singularity. However, they do not possess a foliation as an isolated object in an asymptotically cosmological spacetime. We therefore dismiss them as unphysical.

We examine the global geometry of the corresponding monopole spacetimes when  $M < 0$ . When  $\eta > M_p$ , the exterior spacetime possesses a cosmological horizon. We construct explicitly the Kruskal-Szekeres coordinate system which is non-singular on this horizon. The maximal extension of the exterior geometry is then presented. To provide a physical description of the exterior spacetime we identify explicitly a foliation of this geometry which corresponds to an isolated object in an asymptotically cosmological spacetime.

---

<sup>1</sup>For convenience, we introduce  $M_p \equiv m_p/\sqrt{8\pi}$ .

The paper is organized as follows: In Sec. II, we write down the Einstein equations for our model. In Sec. III, the simpler problem of wall motion in Minkowski space is discussed. In Sec. IV, we examine the motion of the wall coupled to gravity and describe all possible trajectories. In Sec. V, we trace the wall trajectory in spacetime. In Appendix A, the wall equation of motion is analysed in detail in a simple tractable special case. In Appendix B, the routing of the wall trajectories on Kruskal-Szekeres and Gibbons-Hawking diagrams is determined.

## II. EINSTEIN'S EQUATIONS AT THE WALL

The simplest model that admits global monopoles is described by the Lagrangian

$$\mathcal{L} = -\frac{1}{2}\partial_\mu\phi^a\partial^\mu\phi^a - \frac{1}{4}\lambda(\phi^a\phi^a - \eta^2)^2,$$

where  $\phi^a$  is a triplet of scalar fields. The ansatz which describes a static monopole with unit topological charge is (as in Minkowski space)  $\phi^a = \phi(R)\hat{x}^a$ , where  $\hat{x}^a$  is a radial unit vector. The corresponding spacetime is spherically symmetric.

At the center of the monopole, the field is in the false vacuum,  $\phi = 0$ , with energy density  $\rho = \frac{1}{4}\lambda\eta^4$  and pressure  $P = -\rho$ . We will approximate the core of radius  $r$  by a region of false vacuum. The interior spacetime is then de Sitter space, which we can describe by the static line element,

$$ds^2 = -A_D dT_D^2 + A_D^{-1} dR^2 + R^2 d\Omega^2, \quad (2.1)$$

where

$$A_D = 1 - H^2 R^2, \quad H^2 = \frac{8\pi G}{3}\rho. \quad (2.2)$$

The static chart will describe the interior if  $HR < 1$  everywhere.

Asymptotically,  $\phi \approx \eta$ . The stress tensor assumes the perfect fluid form with  $P = -\rho_{\text{ext}}(R)$  where  $\rho_{\text{ext}}(R) \approx \eta^2/R^2$ . The corresponding spacetime is described by the line element (1.1). Harari and Lousto's numerical calculations show that the asymptotic form

(1.1) is approached rapidly outside the core. We will approximate the solution everywhere outside the core by this asymptotic form.

The exterior geometry will be static only if  $\eta < M_p$ . When this limit is breached, the region  $R > -2M/(\eta^2/M_p^2 - 1)$  will assume a dynamical character. Strictly speaking, this is inconsistent with the static ansatz we exploit to generate the asymptotic form of the metric. To resolve this inconsistency we must re-interpret the original ansatz as a description of a dynamical object. What has happened is that the timelike Killing vector which characterizes a static geometry has become spacelike. The radial vector, however, remains normal to the Killing vector. The cosmological nature of the exterior geometry will be described more fully in Sec. V.

The continuity of the lapse and its first derivative across the core boundary determines the equilibrium values (1.3) and (1.4). We note that the maximum core size covered by a static chart is given by  $HR = 1$ . This limit obtains when  $\eta = \sqrt{3}M_p$ . We conclude that a static interior is possible well into the regime  $\eta > M_p$ .

Now let us include a surface energy density on the core boundary. In the thin wall approximation, we can exploit Gaussian normal coordinates adapted to the wall to express the stress tensor there in the form

$$T^a_b = \sigma \delta(n) \delta^a_b. \quad (2.3)$$

$\sigma$  is the constant surface energy density of the boundary. The parameter  $n$  appearing in Eq. (2.3) is the proper distance normal to the worldsheet of the wall. The metric induced on the wall is given by

$$ds^2 = -d\tau^2 + r(\tau)^2 d\Omega^2,$$

where  $\tau$  is the proper time registered by an observer at fixed  $\theta$  and  $\varphi$  who moves with the wall. The problem reduces to the determination of the trajectory,  $r = r(\tau)$ .

The origin of the surface energy density are the field gradients interpolating between the false vacuum interior and the exterior. We approximate it

$$\begin{aligned}\sigma &\sim r_w \times \text{energy density difference} \\ &\sim r_w (\rho - \eta^2/r_w^2)\end{aligned}$$

where  $r_w$  is the size of the monopole. The numerical results of Ref. [7,4] show that  $r_w$  is proportional to  $1/\eta$ . The above relation becomes

$$\sigma \simeq s\eta^3, \quad (2.4)$$

where  $s$  is a dimensionless constant.

The surface energy distribution (2.3) introduces a discontinuity in the spacetime metric at the wall. The Einstein equations at the core boundary reduce to the form [10–12]

$$K^a_b(\text{out}) - K^a_b(\text{in}) = -4\pi\sigma G\delta^a_b, \quad (2.5)$$

where  $K_{ab}(\text{in})$  and  $K_{ab}(\text{out})$  are respectively the extrinsic curvature of the wall embedded in de Sitter space and in the exterior spacetime described by (1.1). Using the techniques developed in [11] or [12], we find that

$$K_{\theta\theta}(\text{in}) = r\beta_D, \quad K_{\theta\theta}(\text{out}) = r\beta_M.$$

Here,  $\beta_D$  and  $\beta_M$  are given by

$$\beta_D = -A_D \dot{t}_D, \quad \beta_M = A_M \dot{t}_M,$$

where  $t_D(\tau)$  and  $t_M(\tau)$  are the de Sitter and exterior ‘static’ time variables,  $T_D$  and  $T_M$  evaluated on the wall. The overdots refer to derivatives with respect to proper time. We recall that [11]

$$\beta_D^2 = A_D + \dot{r}^2, \quad \beta_M^2 = A_M + \dot{r}^2.$$

Now the  $(\theta\theta)$  component of Eq. (2.5) reads

$$\beta_D - \beta_M = 4\pi G\sigma r. \quad (2.6)$$

This equation can be cast in the form,

$$\dot{r}^2 + U(r) = -1, \quad (2.7)$$

where

$$U(r) = -\left(\frac{F_-}{r^2}\right)^2 - H^2 r^2, \quad (2.8)$$

or, alternatively,

$$U(r) = -\left(\frac{F_+}{r^2}\right)^2 - \frac{2GM}{r} - 8\pi G\eta^2, \quad (2.9)$$

with

$$F_{\pm}(r) = \frac{M}{4\pi\sigma} - \frac{\rho_{\pm}}{3\sigma}r^3 + \frac{\eta^2}{\sigma}r, \quad \rho_{\pm} = \rho \pm 6\pi G\sigma^2. \quad (2.10)$$

The linear term in  $F_{\pm}$  encodes completely the topology of the scalar field.

### III. WALL MOTION IN MINKOWSKI SPACE

In the limit  $G \rightarrow 0$ , the Einstein equations should reproduce the description of a global monopole in Minkowski space. In this section, we examine a model of a monopole in Minkowski space. This is a useful preliminary step before attempting to examine Eq. (2.7) in all its glory.

Let the core radius be  $r$ . The energy density in the core is a constant,  $\rho$ , and that in the exterior  $\sim \eta^2/R^2$ . A surface layer with energy density,  $\sigma$ , is located on the core boundary. The total energy of a static configuration is then given by

$$E = \frac{4\pi}{3}\rho r^3 + 4\pi\sigma r^2 + 4\pi\eta^2(R^* - r), \quad (3.1)$$

where  $R^*$  is a cutoff. It is clear that an equilibrium exists. We minimize  $E$  with respect to  $r$  to obtain the stable equilibrium core size,

$$r_0 = -\frac{\sigma}{\rho} + \sqrt{\left(\frac{\sigma}{\rho}\right)^2 + \frac{\eta^2}{\rho}}. \quad (3.2)$$

The (subtracted) energy,  $E^* \equiv E - 4\pi\eta^2 R^*$  is then given by



$$E_0^* = M_0 = -\frac{4\pi}{3} \frac{\sigma^2 r_0}{\rho} \left( 1 + 2 \frac{\rho \eta^2}{\sigma^2} - \sqrt{1 + \frac{\rho \eta^2}{\sigma^2}} \right). \quad (3.3)$$

We note that  $M_0$  is manifestly negative. In the limit  $\sigma \rightarrow 0$ , we have  $r_0 = \frac{\eta}{\sqrt{\rho}}$  and  $E_0^* = -\frac{8\pi}{3} \frac{\eta^3}{\sqrt{\rho}}$ . If we identify  $E^*$  with  $M$ , we reproduce the values obtained by Harari and Lousto which are independent of  $G$ .

More generally, let us examine the motion of the core boundary. The classical action describing this motion is given by

$$S = \int dt \left[ \frac{4\pi}{3} \rho r^3 + 4\pi \sigma r^2 \sqrt{1 - \left( \frac{dr}{dt} \right)^2} + 4\pi \eta^2 (R^* - r) \right]. \quad (3.4)$$

The canonical conserved energy is given by a Legendre transformation of the Lagrangian appearing in Eq. (3.4),

$$E^* = \frac{4\pi}{3} \rho r^3 + 4\pi \sigma r^2 \sqrt{1 + \dot{r}^2} - 4\pi \eta^2 r. \quad (3.5)$$

The only change with respect to Eq. (3.3) is that the boundary term picks up kinetic energy,  $4\pi \sigma r^2 \rightarrow 4\pi \sigma r^2 \sqrt{1 + \dot{r}^2}$ . We can recast Eq. (3.5) in the form

$$\sqrt{1 + \dot{r}^2} = \frac{F}{r^2}, \quad (3.6)$$

where  $F$  is given by

$$F = \frac{E^*}{4\pi\sigma} - \frac{\rho}{3\sigma} r^3 + \frac{\eta^2}{\sigma} r.$$

Eq. (3.6) implies that  $F$  must be positive on any physical trajectory. This condition places a constraint on the extent of the radial domain of the wall.

When  $\dot{r}^2 \ll 1$ , the motion is well described by the potential appearing on the RHS of Eq. (3.1). Clearly, the equilibrium configuration has  $r = r_0$  given by Eq. (3.2) with energy,  $M_0$ , given by Eq. (3.3). In general, we can cast Eq. (3.6) in the form

$$\dot{r}^2 + U(r) = -1,$$

where

$$U(r) = - \left( \frac{F}{r^2} \right)^2. \quad (3.7)$$

This is exactly the limit  $G \rightarrow 0$  of Eq. (2.7) when  $E^*$  is identified with  $M$ . We will examine the solutions admitted by this system with our eye on the analogy with the general relativistic problem.

Let us first examine  $M < 0$ .

We first determine where  $F$  is positive. We note that for each negative value of  $M$  above some lower threshold,  $M_c$ , the cubic function  $F$  has two positive roots,  $r_1$  and  $r_2$  say, and  $F$  is positive only in the domain  $[r_1, r_2]$  — physical motion is necessarily bounded. To determine  $M_c$ , we observe that when  $M$  falls to  $M_c$ , the two roots coalesce with the local maximum. Thus  $F = 0$  and  $F' = 0$  simultaneously. We find that this occurs at  $r = r_c = \frac{\eta}{\sqrt{\rho}}$  and

$$M_c = -\frac{8\pi}{3} r_c \eta^2. \quad (3.8)$$

Below  $M_c$ ,  $F$  is negative everywhere. Therefore  $M = M_c$  places a lower bound on the mass spectrum.

It is now simple to construct the potential,  $U$ , in the regime  $M_c < M < 0$ . We note that  $r^5 U' = -2F(rF' - 2F)$ .  $U$  possesses two maxima coinciding with the roots of  $F$  at  $r_1$  and  $r_2$ . It possesses a single minimum given by the single positive root of the cubic,  $rF' - 2F$ .

On a physical trajectory,  $U \leq -1$ . The static solution with  $U(r) = -1$  at its minimum determines the sharp lower bound,  $M_0$  given by Eq. (3.3), on the mass. We note that  $r_0 < r_c$ . It is then simple to see that  $M_c < M_0$  for all  $\eta$ . The existence of the threshold,  $M_c$ , places no constraint on the spectrum of oscillating solutions.

For each  $M_0 < M < 0$ ,  $r$  will oscillate between two turning points,  $r_{\text{Min}}$  and  $r_{\text{Max}}$ , bounded within the interval,  $[r_1, r_2]$ . This solution will be stable. If initially the core is displaced from equilibrium it will oscillate about the equilibrium. In a physical monopole, we would expect the core to relax to  $r_0$  as the monopole radiates away its excess energy.

The potential  $U(r)$  is plotted in Fig. 1 for a negative value of  $M$ .

While both collapsing and expanding solutions appear to exist in the region outside the interval,  $[r_1, r_2]$ ,  $F < 0$  there. Such solutions are not consistent with the boundary conditions

which correspond to a monopole. They correspond instead to an unphysical inside-out monopole with an interior with energy density,  $\eta^2/R^2$  and an exterior false vacuum. It is simple to check that  $F$  now appears in Eq. (3.6) with a minus sign.

If  $M \geq 0$ ,  $F$  is positive in some finite domain containing the origin. This places a bound on the physical domain of  $r$ .  $U$  increases monotonically over this domain. The core always collapses in a finite proper time,  $\tau_0$ , with  $r \sim (\tau_0 - \tau)^{1/3}$ .

To summarize, in Minkowski space we saw that the spectrum of physically realized values of  $M$  was bounded from below by  $M_0$ . For each  $M_0 \leq M < 0$ , there is a stable oscillating solution and such oscillating solutions exist for all values of  $\eta$ . If  $M \geq 0$  there is a bounded solution which collapses. The only possible motion in Minkowski space is bounded.

#### IV. WALL MOTION

In this section, we discuss the wall motion in general relativity. As we will see, when gravity is turned on the situation can be quite different. In addition to determining the energy density in the interior and on the core boundary  $\eta$  also determines the angle deficit in the exterior.

We would expect the interior to inflate when the core radius exceeds the de Sitter horizon radius. On dimensional grounds this occurs when  $\eta \gtrsim M_p$ . Is this a necessary condition?

If  $\eta < M_p$ , the deficit  $\Delta\Omega < 4\pi$ . Thus, if  $M \geq 0$ , we would expect to reproduce at least qualitatively, the behavior of a false vacuum bubble discussed in [11]. However, while a false vacuum bubble with  $M > 0$  always collapses in Minkowski space, when gravity is taken into account its interior may inflate for any value of the symmetry breaking scale without destroying the exterior and therefore without any violation of flat space intuition in that region. This is because the inflation occurs behind the event horizon of the exterior Schwarzschild geometry. The inflating interior is connected by a wormhole behind this horizon. The event horizon signals the eventual formation of a black hole. All false vacuum bubbles are singular. If  $M < 0$ , unlike the  $M > 0$  Schwarzschild geometry, the exterior

geometry is globally static and there is no exterior horizon. One would not expect to find inflating solutions, singular or otherwise. We will demonstrate explicitly that one does not.

When  $\eta > M_p$ ,  $\Delta\Omega > 4\pi$ . If, in addition,  $M < 0$  the causal roles of  $R$  and  $T_M$  in Eq. (1.1) are interchanged beyond some finite value of  $R$ . This value separates a static region from an expanding cosmological one. This expanding region can support an inflating interior:  $r$  can grow large without doing so at the expense of the monopole exterior.

While  $\eta \gtrsim M_p$  is a necessary condition, it is not a sufficient condition. We have already observed in Sec. II that non-inflating solutions appear to exist when  $\eta \gtrsim M_p$  — they certainly do if  $\eta$  is not too large in the  $\sigma \rightarrow 0$  limit. So  $\eta \gtrsim M_p$  is clearly not a sufficient condition. We will demonstrate explicitly, however, that there is a critical value of  $\eta$  above which all solutions inflate.

Whereas  $F$  was positive in Minkowski space, its relevant general relativistic extensions need not be: as demonstrated in Appendix B,  $F_-$  assumes negative values along physical trajectories when the core is larger than a de Sitter horizon;  $F_+$  may be negative if the Barriola-Vilenkin geometry possesses a horizon.

In this section, we will examine the solution of Eq. (2.7). The determination of the physical spacetime which corresponds to these solutions, and whether they are physically realizable, will require the evaluation of the sign of  $F_-$  and  $F_+$ . This will be deferred to the next section.

It is convenient to introduce dimensionless variables. We define

$$z = Hr, \quad m = \frac{\sqrt{\lambda/3}}{8\pi} \frac{M}{M_p}, \quad \tilde{\rho}_{\pm} = \frac{1}{\eta^2 H^2} \rho_{\pm}. \quad (4.1)$$

Let  $\tilde{\eta} = \eta/M_p$  and  $\tilde{\lambda} = \lambda/3s^2$ . We then have  $F_{\pm} = H^{-2}\mathcal{F}_{\pm}$ , where

$$\mathcal{F}_{\pm} = \frac{1}{2} \tilde{\lambda}^{1/2} \tilde{\eta} \left( m - \frac{\tilde{\rho}_{\pm}}{3} z^3 + z \right), \quad \tilde{\rho}_{\pm} = 3(\tilde{\eta}^{-2} \pm \tilde{\lambda}^{-1}). \quad (4.2)$$

The potential,  $U$ , is now parametrized by three dimensionless parameters:  $\tilde{\eta}$  and  $\tilde{\lambda}$  which characterize the physical theory, and the (reduced) gravitational mass,  $m$ .

$$U = - \left( \frac{\mathcal{F}_-}{z^2} \right)^2 - z^2 = - \left( \frac{\mathcal{F}_+}{z^2} \right)^2 - \frac{m\tilde{\eta}^2}{z} - \tilde{\eta}^2. \quad (4.3)$$

We will consider a theory with a fixed value of  $\tilde{\lambda}$  and examine the behavior as  $\tilde{\eta}$  is dialled from 0 to infinity.

Let us first examine the global properties of the function,  $U$ . As we will see, there are important respects in which the functional form of  $U$  differs from that of its Minkowski space counterpart. To begin with, we note that  $U \leq 0$ . As  $z \rightarrow 0$ ,

$$U \sim -\frac{m^2}{z^4}, \quad (4.4)$$

independent of  $G$ . As  $z \rightarrow \infty$ <sup>2</sup>,

$$U \sim -\left[\left(\frac{\tilde{\rho}_-}{3}\right)^2 + 1\right] z^2. \quad (4.5)$$

From its asymptotics, it is clear that  $U$  always possesses at least one positive maximum. Here we would like to determine the physical conditions under which it may possess additional positive critical points. Specifically, when does it possess a well? Recall that in Minkowski space this occurs when  $M_c < M < 0$ , where  $M_c$  is defined by Eq. (3.8).<sup>3</sup>

In general, at a critical point of  $U$ ,  $U' = 0$  or

$$\frac{\tilde{\lambda}\tilde{\eta}^2}{4}(z + m - \frac{\tilde{\rho}_-}{3}z^3)(z + 2m + \frac{\tilde{\rho}_-}{3}z^3) = z^6. \quad (4.6)$$

We find that, for each  $\tilde{\eta}$  there exists a critical negative mass,  $m_c$ , below which Eq. (4.6) possesses a single positive solution, corresponding to a single maximum for  $U$ . For negative  $m > m_c$ , the equation possesses three positive solutions,  $z_-$ ,  $z_0$  and  $z_+$ : two maxima,  $z_-$  (left) and  $z_+$  (right), and a minimum  $z_0$  lying between them. As  $m$  is lowered to  $m_c$ , the right hand maximum coalesces with the minimum and they annihilate. Let this value be  $z_c$ .

---

<sup>2</sup>We note that  $U \leq -z^2$ , with equality at points where  $\mathcal{F}_- = 0$ , if they exist.

<sup>3</sup>In analogy with the Minkowski space treatment, it is clear that a sufficient condition that it possesses two (or more) maxima is that  $\mathcal{F}_-$  possesses two zeros. There is clearly then (at least) one minimum between them. This is not, however, a necessary condition.

To determine  $m_c$ , we note that when  $m = m_c$ , in addition to  $U' = 0$ , we also have  $U'' = 0$  at this point. We can express these two conditions in the following form

$$m_c = \frac{3}{2} \frac{z_c}{3 - \tilde{\rho}_- z_c^2} (\tilde{\rho}_+^2 z_c^4 - 3) , \quad (4.7)$$

where

$$\tilde{\rho}_+^2 (8\tilde{\rho}_+^2 + \tilde{\rho}_-^2) z_c^8 - 18\tilde{\rho}_- \tilde{\rho}_+^2 z_c^6 - 3(\tilde{\rho}_+^2 - \tilde{\rho}_-^2) z_c^4 - 18\tilde{\rho}_- z_c^2 - 9 = 0 . \quad (4.8)$$

There is a unique positive solution to Eq. (4.8) for each specification of  $\tilde{\eta}$ . Eq. (4.7) then determines  $m_c$ . This solution is given by the line labelled  $m_c$  in the parameter space  $(\tilde{\eta}, m)$  in Fig. 2. Clearly  $m_c < m < 0$  represents a necessary condition for a stable oscillating solution.

We have now determined how the number of critical points of the potential depends on  $m$ .

A necessary condition for classical motion is that  $U \leq -1$ . For a given set of parameters, this condition will partition the domain of  $U$  into allowed (or physical) and forbidden subdomains. This partition, as well as the qualitative nature of the motion in the disjoint physical domains, is completely determined once we know where the critical points of  $U$  lie with respect to its turning points with  $U = -1$ . Let us locate the mass values at which critical points coincide with turning points.

The two equations,  $U = -1$  and  $U' = 0$  can be reduced to a form analogous to (4.7) and (4.8):

$$m = \frac{z}{3z^2 - 2} \left[ 1 - \left( 2 - \frac{1}{3} \tilde{\rho}_- \right) z^2 \right] , \quad (4.9)$$

where

$$(z^2 - 1)(\tilde{\rho}_- z^2 - 1)^2 + \frac{4}{\tilde{\lambda} \tilde{\eta}^2} z^2 (3z^2 - 2)^2 = 0 . \quad (4.10)$$

The solutions are traced on the parameter space in Fig. 2 where they are labelled  $m_0$ ,  $m_+$  and  $m_M$ .

Let us describe these solutions in greater detail:

If  $m_c < m < 0$ , we know that there are three critical points and the potential possesses a well. Under what conditions will a stable oscillating solution exist in this well? In general, we note that the left hand maximum is always the absolute maximum:

$$U(z_-) > U(z_+). \quad (4.11)$$

A stable oscillating solution will therefore exist if the motion is bounded by the right hand maximum,

$$U(z_+) > -1, \quad (4.12)$$

and the minimum lies within the physically accessible domain of  $z$ ,

$$U(z_0) \leq -1. \quad (4.13)$$

Eq. (4.13) is saturated along  $m_0$  on Fig. 2. The mass spectrum of stable oscillations is bounded from below by  $m_0$ . There is a single stationary solution of size  $z_0$ .

If  $\tilde{\eta} < 1$ , Eq. (4.12) is always satisfied. If  $\tilde{\eta} \geq 1$ , however, Eq. (4.12) is saturated along  $m_+$ . Oscillating solutions of arbitrarily small negative mass exist when  $\tilde{\eta} < 1$  but do not when  $\tilde{\eta} > 1$ . If  $\tilde{\eta} < 1$ , the mass spectrum is bounded from above by  $m = 0$ ; if  $\tilde{\eta} \geq 1$ , the spectrum is bounded from above by  $m_+$ .

This behavior can be accounted for analytically. When  $m \rightarrow -0$ , the left maximum at  $z_-$  and the minimum at  $z_0$  degenerate to  $z = 0$  with  $U(z_-) = 0$  and  $U(z_0) \rightarrow -\infty$ . In this limit, Eq. (4.6) determines the position of the right hand maximum  $z_+$ ,

$$\lim_{m \rightarrow -0} z_+^4 = \frac{1}{4} \frac{\tilde{\lambda} \tilde{\eta}^2}{1 + \frac{1}{36} \tilde{\lambda} \tilde{\eta}^2 \tilde{\rho}_-^2}.$$

The condition, (4.12) then determines the limit,  $\tilde{\eta} < 1$ . This is independent of  $\tilde{\lambda}$ . So for infinitesimally small and negative mass, oscillations exist only when  $\tilde{\eta} < 1$ .

Both  $m_0$  and  $m_+$  decrease monotonically with  $\eta$ . They terminate at the common point  $P$  where they coincide with  $m_c$ . This end point defines a critical value of  $\tilde{\eta}$ ,  $\tilde{\eta}_c$ , above

which there do not exist any stable oscillating solutions. Whereas in Minkowski space, the boundary  $m_c$  possesses no physical significance, here it plays a role in the bifurcation in parameter space at  $\tilde{\eta} = \tilde{\eta}_c$ . We note that in the limit  $\sigma \rightarrow 0$ ,  $\tilde{\eta}_c \rightarrow \sqrt{3}$  consistent with the static limit of the de Sitter interior discussed in Sec. II. This, of course, is a highly singular limit.

There is no solution analogous to  $m_+$  for  $z_-$ . This is because  $U(z_-) > -1$  in this regime.

Both when  $m < m_c$  and  $m > 0$ , there is a single maximum  $z_M$  of  $U$ . The condition  $U(z_M) = -1$  identifies a mass,  $m_M$ . See Fig. 2. If  $m < 0$  ( $m > 0$ ), motion is monotonic when  $m < m_M$  ( $m > m_M$ ).  $m = m_M$  therefore identifies the boundary in parameter space separating regimes of monotonic and non-monotonic motion. We note that along the positive branch,  $m_M \rightarrow \infty$  as  $\tilde{\eta} \rightarrow 0$ .

We summarize as follows:

The boundaries  $m_c$ ,  $m_0$ ,  $m_+$ ,  $m_M$  and  $m = 0$  partition the parameter space into seven regions labelled (1) to (7) in Fig. 2.

In the parametric region (1) bounded by  $m = m_0$ ,  $m = m_+$  and  $m = 0$  the potential possesses oscillating, collapsing and expanding domains. This potential is plotted in Fig. 3.1.

In regions (2)-(4), only collapsing and expanding domains exist. In region (2), while the potential does possess a well, its minimum is inaccessible classically. See Fig. 3.2. There are no oscillatory solutions. In region (3), the potential again possesses a well. However, the right maximum no longer provides a barrier containing the motion in the well. Motion in the well is unstable towards expansion. See Fig. 3.3. In region (4), the potential possesses a single classically inaccessible maximum (see Fig. 3.4) which separates collapsing from expanding domains.

In region (5), the single maximum of the potential is accessible. The wall trajectory is monotonic (See Fig. 3.5).

For  $m > 0$ , the potentials in region (6) and (7) are qualitatively identical to those in region (4) and (5) respectively. See Fig. 3.6 and Fig. 3.7. If  $\tilde{\eta} < 1$ , the motion in these



regimes is qualitatively identical to that of the false vacuum bubbles discussed in Ref. [11].

In the next section, we will construct the spacetime which corresponds to each of these trajectories.

The above analysis simplifies considerably if we assume  $\tilde{\rho}_- = 0$  for all  $\tilde{\eta}$  and  $\tilde{\lambda}$ . As we will demonstrate in Appendix A, the overall picture is qualitatively identical to the  $s = \text{constant}$  case.

## V. EMBEDDING THE WALL TRAJECTORIES IN SPACETIME

In this section, we trace the wall trajectory in spacetime.

If  $\tilde{\eta} < 1$ , the exterior metric (1.1) does not possess a horizon. The singularity at  $R = 0$  is a naked one. However, if we truncate the exterior spacetime at some finite value of  $R$  and replace it by a non-singular patch of de Sitter space the singularity is removed. The physical spacetime is free of singularities. The static coordinate system,  $(R, T_M)$ , is globally valid in the exterior.  $T_M$  is the asymptotic time and  $\dot{t}_M$  must be positive along physical trajectories. Just as in the Minkowski space analysis, the sign of  $\dot{t}_M$  is the sign of  $F_+$ . So  $F_+$  must be positive everywhere along trajectories. In Appendix B. we show that  $F_+$  is positive along the oscillatory solution and negative along the others. The only physical solutions are oscillatory. It is simple to check that  $z < 1$  everywhere along these trajectories. The interior is completely covered by a static patch of de Sitter space. It therefore does not inflate. A remote observer will eventually see this stable oscillating motion of the wall. The remaining trajectories correspond to unphysical inside-out solutions. This is completely analogous to the Minkowski space model discussed in Sec. III.

If  $\tilde{\eta} > 1$ , the surface  $R = r_H = 2GM/(1 - \tilde{\eta}^2)$  is null. The coordinate system Eq. (1.1) breaks down at  $R = r_H$ . If  $R < r_H$ , the killing vector  $\partial_{T_M}$  is timelike, and the spacetime is static; if  $R > r_H$ ,  $\partial_{T_M}$  is spacelike. The spacetime is dynamical in this region. At large values of  $R$ , the spacetime metric can be approximated by

$$ds^2 = \frac{-dR^2}{\tilde{\eta}^2 - 1} + (\tilde{\eta}^2 - 1)dT_M^2 + R^2 d\Omega^2. \quad (5.1)$$

As discussed in [13], each constant  $T_M$  slice of the asymptotic geometry is a  $2 + 1$  dimensional Friedman - Robertson - Walker universe expanding linearly with time,  $R$ . The asymptotic geometry can be represented locally by a spherical cylinder  $S^2 \times R$ . This is a highly anisotropic cosmology.

We can introduce Kruskal-Szekeres coordinates,  $(u, v)$  that cover the complete exterior spacetime. The maximal extension of this coordinate system is the spacetime shown in Fig. 4. This spacetime is represented by a subset of a plane, to each point of which corresponds a two-sphere of radius  $R$ . This plane divides naturally into four quadrants. The coordinates are defined as follows in terms of the ‘static’ coordinates in each of these quadrants: in quadrants I and III (upper sign for quadrant I),

$$\begin{aligned} u &= \pm \left(1 - \frac{R}{r_H}\right)^{1/2} \exp\left(\frac{R}{2r_H}\right) \cosh\left(\frac{T_M}{t_1}\right), \\ v &= \pm \left(1 - \frac{R}{r_H}\right)^{1/2} \exp\left(\frac{R}{2r_H}\right) \sinh\left(\frac{T_M}{t_1}\right); \end{aligned}$$

in quadrants II and IV (upper sign for quadrant II),

$$\begin{aligned} u &= \pm \left(\frac{R}{r_H} - 1\right)^{1/2} \exp\left(\frac{R}{2r_H}\right) \sinh\left(\frac{T_M}{t_1}\right), \\ v &= \pm \left(\frac{R}{r_H} - 1\right)^{1/2} \exp\left(\frac{R}{2r_H}\right) \cosh\left(\frac{T_M}{t_1}\right), \end{aligned}$$

where  $t_1 = r_H^2/GM$ . We have

$$\begin{aligned} u^2 - v^2 &= \left(1 - \frac{R}{r_H}\right) \exp\left(\frac{R}{r_H}\right), \\ \frac{v}{u} &= \tanh\left(\frac{T_M}{t_1}\right) \text{ (in I, III)}, \quad \frac{u}{v} = \tanh\left(\frac{R}{t_1}\right) \text{ (in II, IV)}. \end{aligned} \tag{5.2}$$

The spacetime is defined by the region  $u^2 - v^2 \leq 1$  on the  $u$ - $v$  plane.  $R$ -constant lines are hyperbolas which degenerate into straight lines,  $v = \pm u$  on the horizons,  $R = r_H$ . There are two naked singularities given by the timelike hyperbolas,  $u^2 - v^2 = 1$ .  $T_M$ -constant lines are straight lines passing through the origin.

One way to describe the global geometry of this spacetime is to consider a foliation by constant  $v$  hypersurfaces. The spacetime is symmetric with respect to time reversal  $v \rightarrow -v$ .

The hypersurface  $v = 0$  is momentarily static. The topology of this hypersurface is  $S^3$  with singular poles. The equatorial radius is  $r_H$ . As  $v$  is increased, the equatorial radius increases monotonically while the geodesic distance between the poles increases more slowly. While the singularities of the maximally extended geometry are naked, they do not appear on the truncation of this geometry which corresponds to the physical exterior region unless the core originates at or collapses to  $r = 0$ .

The physical exterior region surrounding a global monopole is clearly very different from the global geometry we have just described. Sakai *et al.* have described numerically the evolution of an inflating global monopole in a spacetime which is initially flat. The initial core radius in their model lies outside the monopole horizon. Let us suppose that we place the monopole on the left of the  $u - v$  plane. The maximal extension of such a slice might be approximated by the flat spatial hypersurface,  $\Sigma$  on Fig. 4. It coincides with the hypersurface  $v = 0$  at the point  $(-1, 0)$ , crosses the horizon  $v = -u$  at some finite positive value of  $v$  and tends asymptotically to  $v = u$ . The initial data on the slice will not generally be stationary. The future of this slice lies entirely within the two quadrants (II) and (III). The asymptotic region described by Eq. (5.1) lies completely within region (II). The remaining two quadrants (I) and (IV) are inaccessible for the boundary conditions we are considering. This is analogous to the description of stellar collapse, where half of the maximally extended Schwarzschild geometry gets discarded.

Now let us examine the interior de Sitter space. To trace the trajectory in de Sitter space it is convenient to describe it by Gibbons-Hawking coordinates,  $(U, V)$ . These coordinates have been described elsewhere in detail. We refer the reader to [11] for further details. Briefly, with respect to these coordinates, de Sitter space is represented by the region,  $|U^2 - V^2| \leq 1$  on the  $U - V$  plane, each point of which represents a 2-sphere of radius  $R$ , related to  $U$  and  $V$  by  $U^2 - V^2 = (1 - HR)/(1 + HR)$ . See Fig. 5. The de Sitter horizon of the north (south) pole  $(-1, 0)$   $((1, 0))$  is represented by  $V = U$  ( $V = -U$ ). The center of the monopole is located on the left at the north pole.

The flat slice,  $\Sigma$ , in the maximal extension of the exterior geometry will be truncated

at its intersection with the relevant wall trajectory. It can, however, be extended into the interior. Indeed, the standard presentation of de Sitter space is as a spatially flat Friedman-Robertson-Walker Universe. This slice is labelled  $\Sigma'$  on Fig. 5.  $\Sigma'$  coincides with the hypersurface  $V = 0$  at the point  $(-1, 0)$ , crosses the horizon  $V = -U$  at some finite positive value of  $V$  and tends asymptotically to  $V = U$ . The future of  $\Sigma'$  lies entirely within the two quadrants (II) and (III). Initial data is defined on the union of the interior and exterior flat slices.

The role played by the two fugacities,  $\beta_D$  and  $\beta_M$ , was described in [11] in the context of a Schwarzschild exterior. They demonstrated that  $\beta_D$  ( $\beta_M$ ) was proportional to minus the angular velocity about the origin on a Gibbons-Hawking (Kruskal-Szekeres) spacetime diagram for the interior (exterior) respectively. In Appendix B, we show that the sign of  $\beta_D$  ( $\beta_M$ ) coincides with the sign of  $\mathcal{F}_+$  ( $\mathcal{F}_-$ ). These signs therefore determine uniquely the routing of trajectories about the origins of Figs. 4 and 5. The relevant interior and exterior spacetimes can then be constructed with this information.

Let us first discuss the trajectories of the wall in the exterior.

All oscillating trajectories lie entirely within region (III) on the Kruskal-Szekeres plane. Their trajectories are labelled  $\mathcal{O}$  in Fig. 4.

We describe bounces with the stationary initial condition,  $\dot{r} = 0$ .

There are two qualitatively distinct expanding bounce trajectories. The trajectory, labelled  $\mathcal{B}_{(3)}$  in Fig. 4 (which corresponds to parameters lying within region (3) in Fig. 2), also originates in region (III) though this region need not be part of the physical spacetime. If it is, the exterior possesses a horizon. The bounce may also then have a stationary point within the physical region. It must, however, always cross the horizon and enter region (II). Its motion changes direction at some point outside the horizon which we can set to occur at  $T_M = 0$  without loss of generality. (See Appendix B.) The remaining expanding bounce trajectories,  $\mathcal{B}_{(1),(2),(4)}$ , (corresponding to parameters in regions (1), (2) and (4) on Fig. 2), as well as all monotonically expanding trajectories,  $\mathcal{M}$  (region (5)), originate in the unphysical region (I). They do not possess any physically accessible stationary points. However, they

cross the horizon and enter the physical region (II). There is no horizon in the exterior.

All collapsing trajectories, labelled  $\mathcal{C}$  in Fig. 4 lie entirely within the unphysical region (I). They cannot be realized in an asymptotically cosmological geometry.

As  $\tilde{\eta}$  increases the horizon scale shrinks to zero,  $r_H \rightarrow 0$ , where the exterior geometry is singular. The external metric (1.1) we have been exploiting, based on Barriola and Vilenkin's asymptotic exact solution, is not expected to provide a valid approximation under these circumstances. In particular, in this limit, the description of the region  $R < r_H$  breaks down. However, we also found that oscillating solutions do not exist for large  $\eta$ ; the expanding solution of type  $\mathcal{B}_{(3)}$  is expected to be formed in region (II) with an initial size much larger than  $r_H$ . The analysis of trajectories remains valid.

The expanding type  $\mathcal{B}_{(3)}$  motion is unbounded,  $r \rightarrow \infty$ . However, outside the horizon, the exterior spacetime is itself expanding. After an initial invasive period (to  $T$  on Fig. 4) the expansion of the wall is not at the expense of the ambient exterior. All expanding trajectories move eventually to the left. Therefore, a remote observer in the exterior is safe not to be swallowed by the the expansion of the monopole. This observer will, however, eventually see all trajectories.

In Figs. 5 and 6, we plot the corresponding embedding of possible wall trajectories in de Sitter space.

Oscillating trajectories,  $\mathcal{O}$ , both for  $\tilde{\eta} \geq 1$  and for  $\tilde{\eta} < 1$ , are contained completely within region III on the Gibbons-Hawking plane. The wall does not cross the horizon and the interior does not inflate.

Along the infinite trajectories of type  $\mathcal{B}$  and  $\mathcal{M}$ , however,  $r$  must cross the de Sitter horizon at some point and enter region II. The interior spacetime necessarily inflates. The qualitative nature of these inflating solutions will depend on the magnitude of  $\tilde{\eta}$ . There is a critical value of  $\tilde{\eta}$ ,  $\tilde{\eta}_D = \sqrt{\tilde{\lambda}}$ , below which all inflating trajectories move asymptotically to the left, and above which they all move to the right. Compare Fig. 5 with Fig. 6. Once any constant  $T_D$  hypersurface is breached, it cannot be recrossed. A foliation of de Sitter space by constant  $V$  hypersurfaces reveals that the spherically symmetric inflating region in the

former case ( $\tilde{\eta} < \tilde{\eta}_D$ ) is contained completely in the northern hemisphere of de Sitter space; in the latter ( $\tilde{\eta} > \tilde{\eta}_D$ ) it contains the equator. The volume of the inflating region increases with increased  $\tilde{\eta}$ .

Technically, at the critical value,  $\tilde{\eta} = \tilde{\eta}_D$ ,  $\tilde{\rho}_- = 0$ . If  $\tilde{\eta} > \tilde{\eta}_D$ , then  $\tilde{\rho}_- < 0$ . In appendix B., we demonstrate explicitly how the sign of  $\mathcal{F}_-$  and hence the routing of trajectories is affected. If  $\tilde{\eta} < \tilde{\eta}_D$ ,  $\mathcal{B}_{(3)}$  originates in (III) changes direction outside the de Sitter horizon.  $\mathcal{B}_{(1),(2),(4)}$  and  $\mathcal{M}$  originate in (I). They do not change direction.

If  $\tilde{\eta} > \tilde{\eta}_D$ ,  $\mathcal{B}_{(3)}$  still originates in (III). However, it no longer changes direction outside the de Sitter horizon. We note that  $\tilde{\eta}_D > \tilde{\eta}_c$  so that parameter regions (1) and (2) are not present.  $\mathcal{B}_{(4)}$  now originates in (III). It does not change direction.  $\mathcal{M}$  still originates in (I). However, it now changes direction in (II).

In general, the initial region of de Sitter space bounded by  $\mathcal{B}_{(3)}$  may be smaller than the horizon. That bounded by  $\mathcal{B}_{(4)}$  may also be when  $\tilde{\eta} > \tilde{\eta}_D$ .  $\mathcal{B}_{(1),(2)}$  and  $\mathcal{M}$ , however, always contain a horizon.

## VI. CONCLUSIONS

We have presented a simple model of a global monopole. This model predicts that if  $\tilde{\eta} \equiv \eta/M_p < 1$ , there is always a stable static solution with a negative gravitational mass. There is no inflation. If  $\tilde{\eta} > 1$ , but below some critical value, there exist classically stable analogues of these static monopoles. However, the exterior spacetime is no longer static. For all  $\tilde{\eta} > 1$ , there exist non-singular inflating monopoles with strictly negative gravitational mass.

These inflating solutions differ from the false vacuum bubble solutions examined in [11] in the important respect that the spacetime is non-singular.

The monopole interior inflates when the core radius exceeds the de Sitter horizon radius. Once the wall radius,  $r$ , crosses the horizon it must continue to expand. There are no inflating solutions with constant  $r$ .

In a false vacuum bubble with  $M > 0$ , the inflating interior does not destroy the exterior because it occurs behind the event horizon of the exterior Schwarzschild geometry. In the present case with  $M < 0$ , the picture is very different. There are no horizons when  $\tilde{\eta} < 1$ . But there is no inflation so there is no difficulty reconciling physics in the interior with that in the exterior. However, when  $\tilde{\eta} > 1$  there are inflating monopoles but no wormhole and no event horizon. To understand what is happening, we found it useful to exploit a Kruskal-Szekeres diagram, Fig. 4 to represent the global spacetime structure of the exterior. There is a cosmological horizon,  $v = -u$ , beyond which the spacetime to the future of any spacelike asymptotically flat slice is dynamical. In this region the roles of  $T$  and  $R$  get interchanged. The Schwarzschild parameter,  $T$ , is no longer the proper time of an inertial observer at  $R = \infty$ .  $\partial_{T_M}$  is a spatial Killing vector in this region.  $R$  is time. As  $R \rightarrow \infty$ , the geometry can be represented by a universe expanding linearly with time,  $R$  along two directions. Because of this expansion the unlimited expansion of the core radius is not at the expense of the exterior spacetime. If  $\eta$  is sufficiently large the monopole horizon is small and the core boundary will always be located in the dynamical region. It inflates.

Considering the simplifying assumptions we have made to model the system, the critical value we find,  $\tilde{\eta}_c \approx 1.235$  ( $\eta_c \approx 0.25m_p$ ) agrees well with the value,  $\eta_c \approx 0.33m_p$  determined numerically by Sakai *et al.* [4]. In addition, we note that with a flatter  $\phi^6$  potential, using the numerical technique adapted in [4,13] we obtain the numerical value,  $\eta_c \approx 0.265m_p$  which is closer to our critical value. The flatter the potential the better the thin wall approximation is expected to be.

There are several open questions related to this work that merit further examination.

For each  $\tilde{\eta}$  in the interval,  $1 < \tilde{\eta} < \tilde{\eta}_c$  we saw that a stable oscillating solution co-exists with an expanding solution of the same mass in some strictly negative band of values of  $m$ . It would appear that all non-inflating monopoles are therefore metastable with  $\tilde{\eta} > 1$ : there is the possibility of its tunneling into an inflating configuration. In the semiclassical approximation tunneling will be described by an instanton which interpolates between the oscillating and inflating solutions [12].

A static monopole minimizes the energy within the topological class to which it belongs. We would expect it to be stable against perturbations. It is not so clear what to expect in an inflating monopole. This question can be addressed within the context of the present model by examining the stability of the exterior geometry with respect to perturbations. Formally this problem is almost identical to the analysis of perturbations about a Schwarzschild geometry. However, the exterior is now cosmological, not static, and the boundary conditions involved are very different.

We have only considered global monopoles. It should be straightforward to examine gauge monopoles, as well as cosmic strings and domain walls in this approximation [14].

### ACKNOWLEDGMENTS

This approach to global monopoles was suggested by Alexander Vilenkin and we have benefitted greatly from conversations with him. We also thank Daniel Sudarsky for helpful discussions. JG gratefully acknowledge the hospitality of the Institute of Cosmology at Tufts University, support from CONACyT Grant 211085-5-0118PE and a DGAPA sabbatical fellowship from UNAM.

### APPENDIX A: ANALYSIS OF THE WALL MOTION IN A SIMPLIFIED LIMIT

In this section, we analyze the wall motion in the analytically tractable special case given by  $\tilde{\rho}_- = 0$ .

We note that the reduced energy density difference,  $\tilde{\rho}_-$ , defined by (4.2) is bounded from below by the negative value,  $-3\tilde{\lambda}^{-1}$ . In this regime, the gravitational potential is strong. It has no Minkowski space analogue.  $\tilde{\rho}_-$  diverges to plus infinity as  $\tilde{\eta} \rightarrow 0$ . This is the Minkowski limit.  $\tilde{\rho}_-$  vanishes when  $\tilde{\eta} = \sqrt{\tilde{\lambda}}$ . Remarkably, the potential simplifies on this subset of parameter space deep in the non-perturbative regime. When  $\tilde{\rho}_- = 0$ ,

$$\mathcal{F}_- = \frac{1}{2}\tilde{\eta}^2(m+z) \tag{A1}$$



is linear in  $z$  with slope  $\tilde{\eta}^2/2$ . The necessary condition for classical motion,  $U \leq -1$ , now assumes the particularly simple form

$$|\mathcal{F}_-| \geq \mathcal{G}_s(z), \quad (\text{A2})$$

where

$$\mathcal{G}_s(z) = z^2(1 - z^2)^{1/2}$$

if  $z \leq 1$  and zero otherwise. We note that

$$\mathcal{G}'_s(z) = \frac{z(2 - 3z^2)}{(1 - z^2)^{1/2}}, \quad \mathcal{G}''_s(z) = \frac{2 - 9z^2 + 6z^4}{(1 - z^2)^{3/2}}.$$

The function,  $\mathcal{G}_s$ , has a single maximum at  $z = \sqrt{2/3}$ , an inflection point at  $z_i = \sqrt{(9 - \sqrt{33})/12}$ , and vanishes at  $z = 0$  and  $z = 1$ . The inequality (A2) is very simply illustrated graphically. There are three possibilities. Two intersections of the graphs  $|\mathcal{F}_-|$  and  $\mathcal{G}_s$  indicate the existence of two bounce motions described in the text, one of which collapses the other expands. Four intersections (three with  $\mathcal{F}_-$  and one with  $-\mathcal{F}_-$ ) indicate, in addition, the existence of an oscillating solution lying in the domain between the two bounces. Zero intersection indicates a monotonic solution. We illustrate all three possibilities in Fig. 7.

With  $\tilde{\eta}$  fixed, let us dial  $m$  beginning with  $m = 0$  and decreasing through negative values.

Suppose that  $m$  is small and negative. Only two of the possibilities described above are possible: either there are two or there are four intersections of  $|\mathcal{F}_-|$  and  $\mathcal{G}_s$ . Now when  $m = 0$ ,  $-\mathcal{F}_-$  can intersect  $\mathcal{G}_s$  only at  $z = 0$ .  $\mathcal{F}_-$  also intersects  $\mathcal{G}_s$  at  $z = 0$ . It will re-intersect  $\mathcal{G}_s$  only if its slope lies below some critical value. We find

$$z^4 - z^2 + \left(\frac{\tilde{\eta}^2}{2}\right)^2 \leq 0.$$

There exist two real solutions if and only if the discriminant of the quadratic in  $z^2$  is positive, or  $\tilde{\eta} \leq 1$ . This reproduces the criterion for the existence of a zero mass oscillating solution obtained earlier in our general discussion.

Let  $\tilde{\eta} > 1$ . It is clear that if, in addition,  $\tilde{\eta}$  lies above some critical value  $\tilde{\eta}_c$ ,  $\mathcal{F}_-$  will never intersect  $\mathcal{G}_s$  more than once. This critical value occurs when the slope of  $\mathcal{F}_-$  exceeds the maximum slope of  $\mathcal{G}_s$ . Thus  $\tilde{\eta}_c^2 = 2\mathcal{G}'_s(z = z_i)$ , where

$$\mathcal{G}'_s(z = z_i) = \frac{1}{4}(-1 + \sqrt{33})\sqrt{\frac{9 - \sqrt{33}}{3 + \sqrt{33}}},$$

which gives  $\tilde{\eta}_c \approx 1.203$ .

For all  $\tilde{\eta}$  within the range  $1 \leq \tilde{\eta} \leq \tilde{\eta}_c$ , there will exist some band  $[m_0, m_+]$  within which  $\mathcal{F}_-$  will intersect  $\mathcal{G}_s$  three times. These values are determined by the real solutions of

$$\mathcal{F}_- = \mathcal{G}_s, \quad \mathcal{F}'_- = \mathcal{G}'_s, \quad (\text{A3})$$

satisfying respectively  $\mathcal{G}''_s < 0$ , and  $\mathcal{G}''_s > 0$ . These equations (A3) reduce to Eq. (4.10) and (4.9) on setting  $\tilde{\rho}_- = 0$ . The solution is represented by the lines  $m_0, m_+$  on the  $\tilde{\eta} - m$  plane in Fig. 7. The interpretation is identical to that for the generic case.

A simple bound can be placed on  $m_M$  by inspection. Let the position of intersection of  $-\mathcal{F}_-$  and  $\mathcal{G}_s$  be  $z_M$  when  $m = m_M$ . We have  $m_M = -z_M - 2\mathcal{G}_s(z_M)\tilde{\eta}^{-2}$ . An upper bound is obtained by approximating the position of intersection by  $z = 1$ ,  $m_M < -1$ . A lower bound is obtained by replacing  $\mathcal{G}_s(z_M)$  by the maximum of  $\mathcal{G}_s$  which is  $2\sqrt{3}$ . Thus

$$m_M \geq -1 - \frac{4}{3\sqrt{3}}\tilde{\eta}^{-2}. \quad (\text{A4})$$

The one qualitative difference with the generic case is that  $m_M \rightarrow -\infty$  as  $\tilde{\eta} \rightarrow 0$  along its negative branch. This divergence can be justified as follows: if  $\tilde{\rho}_- = 0$ , the limit  $\tilde{\eta} \rightarrow 0$  implies that  $s \rightarrow \infty$ . A large value of  $s$  corresponds to a large energy density on the surface compared to that in the interior — a situation which is never realized in a monopole.

Finally, we can determine the functional form,  $m_c = m_c(\tilde{\eta})$  exactly. Setting  $\tilde{\rho}_- = 0$ , Eq. (4.8) implies

$$z = \left( \frac{1 + \sqrt{33}}{48} \frac{\tilde{\lambda}\tilde{\eta}^2}{4} \right)^{1/4} = \left( \frac{1 + \sqrt{33}}{192} \right)^{1/4} \tilde{\eta}.$$

Eq. (4.7) then determines

$$m(\tilde{\eta}) = \frac{-15 + \sqrt{33}}{48} \left( \frac{1 + \sqrt{33}}{12} \right)^{1/4} \tilde{\eta},$$

which is linear in  $\tilde{\eta}$  with negative slope, and independent of Newton's constant,  $G$ .

## APPENDIX B: ROUTING OF THE WALL TRAJECTORIES ON KRUSKAL-SZEKERES AND GIBBONS-HAWKING DIAGRAMS

Let us rewrite Eq. (4.3) as

$$\dot{z}^2 = \frac{1}{z^4} (\mathcal{F}_\pm^2 - \mathcal{G}_{M,D}),$$

where

$$\mathcal{G}_M = z^3 [(1 - \tilde{\eta}^2)z - m\tilde{\eta}^2], \quad \mathcal{G}_D = z^4(1 - z^2),$$

and  $\mathcal{F}_\pm$  are given by Eq. (4.2). Classical motion of the wall is allowed only in domains where  $\mathcal{F}_+^2 > \mathcal{G}_M$  or, equivalently,  $\mathcal{F}_-^2 > \mathcal{G}_D$ . Points where  $\mathcal{F}_\pm^2 = \mathcal{G}_{M,D}$ , if they exist, mark the turning points of the motion.

In Sec. V we claimed that the sign of  $\mathcal{F}_+$  and  $\mathcal{F}_-$  determine the routing of the wall trajectory on the Kruskal-Szekeres and Gibbons-Hawking diagrams respectively. To show this (in the former case), we note that Eq. (2.6) - (2.9) relate  $\mathcal{F}_+$  to the fugacity,  $\beta_M$ :  $\mathcal{F}_+ = z^2\beta_M$ . We exploit the definition of  $\beta_M$ , and Eq. (5.2) to give

$$\beta_M = A_M \dot{t}_M = \frac{8G^2M^2}{(1 - 8\pi G\eta^2)^2} \frac{1}{r} \exp\left(-\frac{1 - 8\pi G\eta^2}{2GM} r\right) (\dot{u}v - u\dot{v}).$$

This is independent of the quadrant in question. The change of the polar angle,  $\theta_M = \tan^{-1}(v/u)$ , on the Kruskal-Szekeres plane is

$$\dot{\theta}_M = \frac{u\dot{v} - \dot{u}v}{u^2} \cos^2 \theta_M.$$

Therefore  $\beta_M \sim -\dot{\theta}$ . The sign of  $\mathcal{F}_+$  determines the routing of the trajectory about the origin,  $(0,0)$ . Positive  $\mathcal{F}_+$  corresponding to clockwise motion.

In de Sitter space, we get

$$\beta_D = -A_D \dot{t}_D = -\frac{1}{H}(1 + Hr)^2(U\dot{V} - \dot{U}V) \sim -\dot{\theta}_D,$$

where  $\theta_D = \tan^{-1}(V/U)$  and  $\mathcal{F}_- = z^2\beta_D$ . As before, the sign of  $\mathcal{F}_-$  determines the routing of the trajectory on the Gibbons-Hawking diagram. Positive  $\mathcal{F}_-$ , as for  $\mathcal{F}_+$  implies closewise motion.

If  $\tilde{\eta} < 1$ , there are four distinct regimes in parameter space we need to analyse, labelled (1), (2), (4) and (5) in Fig. 2. We plot both  $\mathcal{F}_+^2$  and  $\mathcal{G}_M$  vs.  $z$  in Fig. 8 for each of these cases in turn.  $\mathcal{G}_M$  is positive everywhere because there is no horizon in the exterior. As we argued in Sec. V. the only physically acceptable values of  $\mathcal{F}_+$  are positive.

In (1),  $\mathcal{G}_M$  intersects  $\mathcal{F}_+^2$  at 4 points. There are 3 disjoint domains where classical motion is allowed. From the left to the right, they correspond to collapsing, oscillating and expanding motion. The sign of  $\mathcal{F}_+$  is positive on the oscillating domain and negative in the others.

In (2),  $\mathcal{G}_M > \mathcal{F}_+^2$  in the central region, indicating that the minimum of the potential well is inaccessible — there are no classically allowed oscillations. However,  $\mathcal{F}_+$  is negative on the two accessible domains.

In (4)  $\mathcal{G}_M$  intersects  $\mathcal{F}_+^2$ ; in (5) it does not (motion is monotonic).  $\mathcal{F}_+$  is negative everywhere in both cases.

If  $\tilde{\eta} > 1$ ,  $\mathcal{G}_M = 0$  when  $R = r_H$ . Whereas Fig. 9 is superficially identical to Fig. 8 for the regimes (1), (2), (4) and (5), the physical interpretation is very different because of the existence of the horizon.

In (1),  $\mathcal{F}_+$  is positive on the oscillating domain. This locates the oscillating trajectory in (III) and not in (I).  $\mathcal{F}_+$  is negative in the remaining domains. The collapsing trajectory necessarily lies in (I). The expanding solution has its stationary point in (I), crosses the horizon and enters (II). See Fig. 4.

In (2) and (4), the collapsing and expanding trajectories are located as in (1) above. In (5), the monotonic trajectory originates at  $r = 0$  in region (I), crosses the horizon and enters (II) exactly like the expanding trajectories in (2) and (4).

All intersections of  $\mathcal{F}_+^2$  with  $\mathcal{G}_M$  lie within the horizon,  $r < r_H$ . Stationary points

necessarily lie in the static region.

In the remaining regime (3), there is an additional feature we have not encountered so far. In the expanding domain,  $\mathcal{F}_+$  changes sign from positive to negative beyond the horizon. This means that the trajectory (labelled  $\mathcal{B}_{(3)}$ ) must change its angular course at some point on the Kruskal-Szekeres plane. Without loss of generality we can always set this value to  $T_M = 0$ . This trajectory evolves closewise prior to this point and counter-clockwise thereafter. See Fig. 4.

Now let us turn inwards. In contrast to  $\mathcal{F}_+$ , the sign of the leading term,  $-\tilde{\rho}_- z^3$  appearing in  $\mathcal{F}_-$ , does depend on the magnitude of  $\eta$ .

If  $\tilde{\rho}_- > 0$  ( $\tilde{\eta} < \sqrt{\tilde{\lambda}}$ ), the functional form of  $\mathcal{F}_-$  is qualitatively identical to that of  $\mathcal{F}_+$  for  $\tilde{\eta} > 1$  and the location of trajectories on the Gibbons-Hawking plane the same as that for the Kruskal-Szekeres plane (Fig. 10).

If  $\tilde{\rho}_- < 0$  ( $\tilde{\eta} > \sqrt{\tilde{\lambda}}$ ), however,  $\mathcal{F}_-^2$  intersects  $\mathcal{G}_D$  twice in regions (3) and (4) (Fig. 11). Unlike the previous case,  $\mathcal{F}_- > 0$  everywhere along the expanding  $\mathcal{B}_{(3)}$  trajectories. The polar angle is monotonic. The stationary point of  $\mathcal{B}_{(4)}$  has moved from (I) into (III). See Fig. 6.  $\mathcal{F}_-$ , on the other hand, now changes sign in the domain,  $z > 1$  along  $\mathcal{M}_{(5)}$ . The corresponding trajectories traced on Fig. 6.

## REFERENCES

- [1] A. Vilenkin and E.P.S. Shellard, Cosmic Strings and Other Topological Defects (Cambridge Univ. Press, Cambridge, 1994)
- [2] A. Vilenkin, Phys. Rev. Lett. **72**, 3137 (1994)
- [3] A. Linde, Phys. Lett. **B327**, 208 (1994)
- [4] N. Sakai, H. Shinkai, T. Tachizawa and K. Maeda, Phys. Rev. **D53**, 655 (1996)
- [5] M. Barriola and A. Vilenkin, Phys. Rev. Lett. **63**, 341 (1989)
- [6] R. Gregory, Phys. Rev. **D54**, 4995 (1996)
- [7] D. Harari and C. Lousto, Phys. Rev. **D42**, 2626 (1990)
- [8] U. Nucamendi and D. Sudarsky, Class. Quantum Grav. **14**, 1309 (1997)
- [9] S. Coleman, Uses of Instantons in ‘The Whys of Sub-Nuclear Physics’ ed. by Zichichi (Plenum Press, New York, 1979)
- [10] W. Israel, Nuovo Cimento **44B**, 1 (1966)
- [11] S.K. Blau, E.I. Guendelman and A.H. Guth, Phys. Rev. **D35**, 1747 (1987)
- [12] E. Farhi, A.H. Guth and J. Guven, Nucl. Phys. **B399**, 417 (1990)
- [13] I. Cho and A. Vilenkin, Phys. Rev. **D56**, 7621 (1997)
- [14] K.G. Zloshchastiev, preprint gr-qc/9708024 OB

# FIGURES

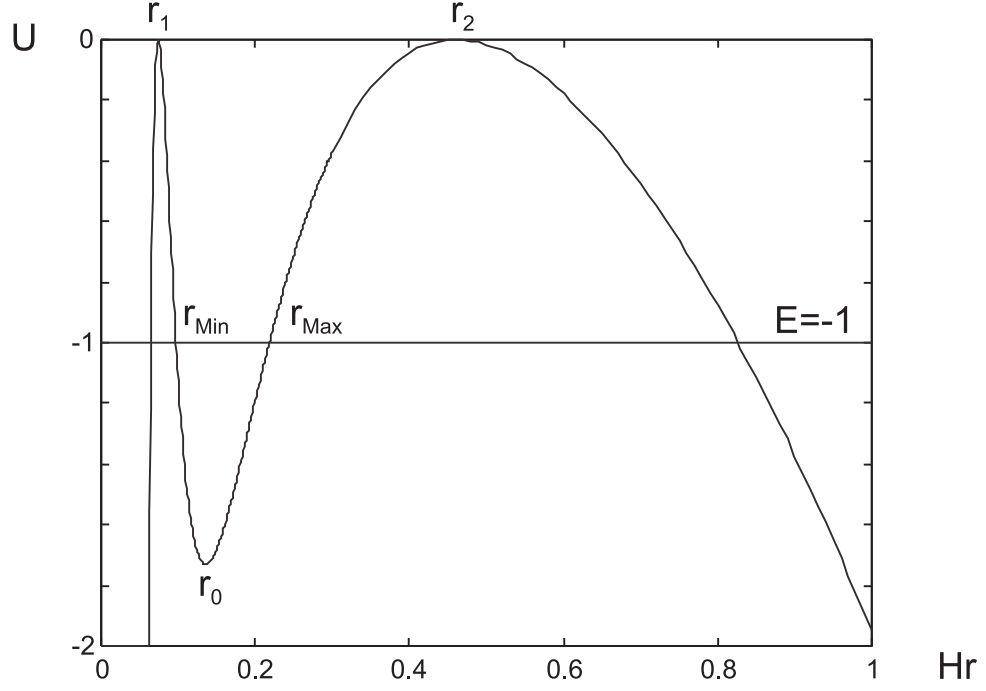
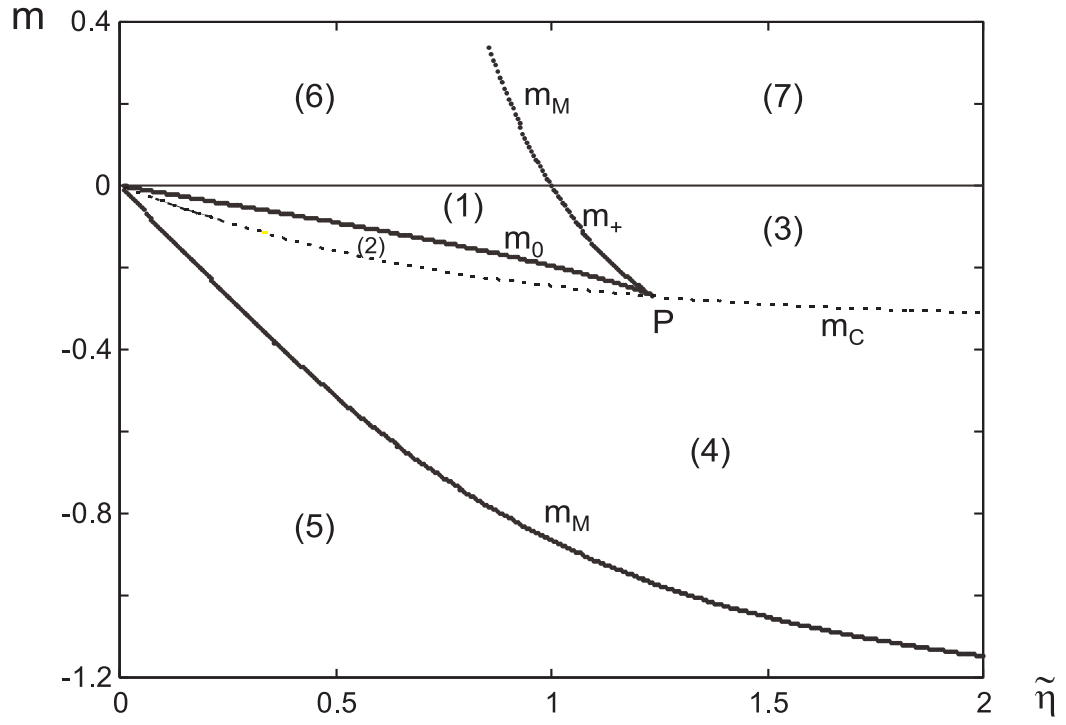
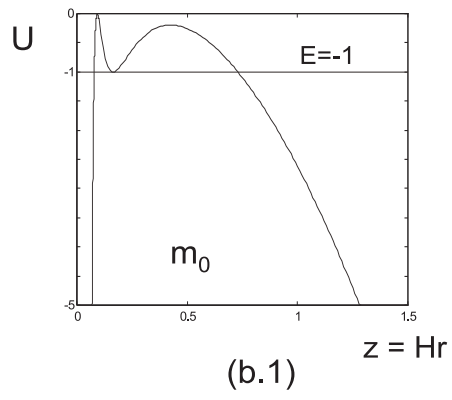


FIG. 1. Plot of  $U(r)$  vs.  $r$  in Minkowski space with  $\eta = 0.1m_p$ ,  $M = -2m_p$ .

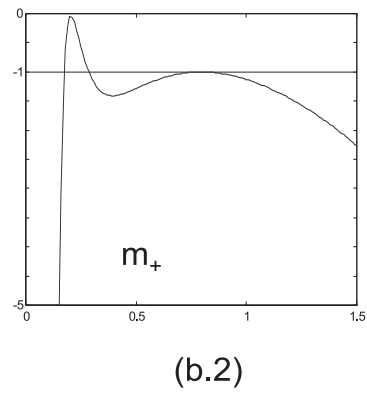
The wall oscillates between a minimum at  $r_{\text{Min}}$  and a maximum at  $r_{\text{Max}}$ . The physical domain of  $U$  is contained within the interval,  $[r_1, r_2]$ , over which  $F$  is positive.



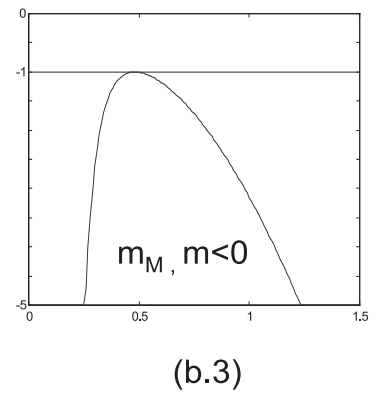
(a)



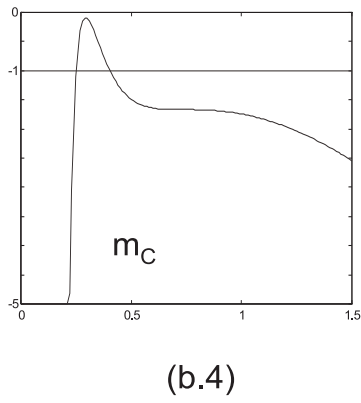
(b.1)



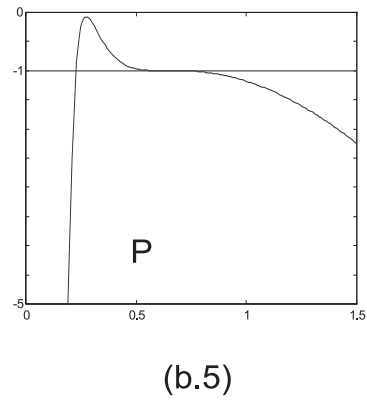
(b.2)



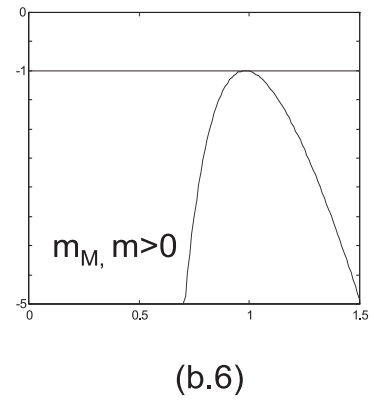
(b.3)



(b.4)



(b.5)



(b.6)



FIG. 2. (a) The parametric space of the model,  $m$  vs.  $\tilde{\eta}$  with  $\tilde{\lambda}(\lambda = 0.1, s = 0.1) = 3.33$ . In the region  $m_c < m < 0$  the potential,  $U$ , possesses two maxima  $z_-$ ,  $z_+$ , and a minimum,  $z_0$  between them. Along  $m_0$ ,  $U = -1$  at  $z_0$ ; along  $m_+$ ,  $U = -1$  at  $z_+$ . In the regions  $m < m_c$  and  $m > 0$ ,  $U$  has a single maximum,  $z_M$ .  $U = -1$  at  $z = z_M$  along  $m_M$ .  $m_0$  and  $m_+$  terminate at the point,  $P$  which lies on  $m_c$ . The boundaries  $m_c$ ,  $m_0$ ,  $m_+$ ,  $m_M$  and  $m = 0$  partition the parameter space into seven regions with qualitatively different potentials. The potentials on these boundaries are plotted in Fig. 2(b). (b.1)  $m_0$  ( $\tilde{\eta} = 0.5$ ,  $m = -0.0896$ ), (b.2)  $m_+$  ( $\tilde{\eta} = 1.15$ ,  $m = -2.006$ ), (b.3)  $m_M$ ,  $m < 0$  ( $\tilde{\eta} = 0.5$ ,  $m = -0.5136$ ), and (b.4)  $m_c$  ( $\tilde{\eta} = 1.57$ ,  $m = -0.2926$ ). (b.5) At  $P$  ( $\tilde{\eta} = \tilde{\eta}_c = 1.235$ ,  $m = -0.2677$ ), (b.6)  $m_M$ ,  $m > 0$  ( $\tilde{\eta} = 0.5$ ,  $m = 2.9212$ ) .

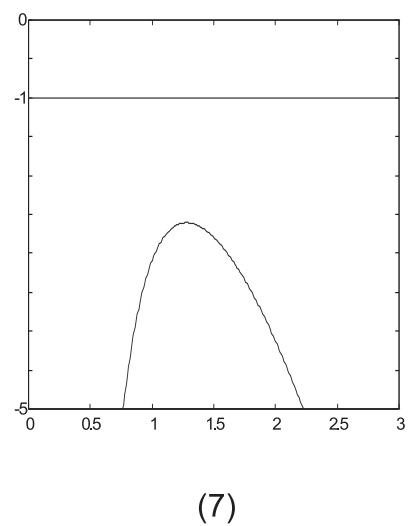
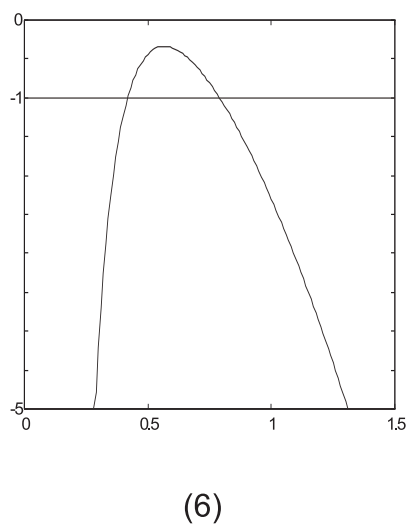
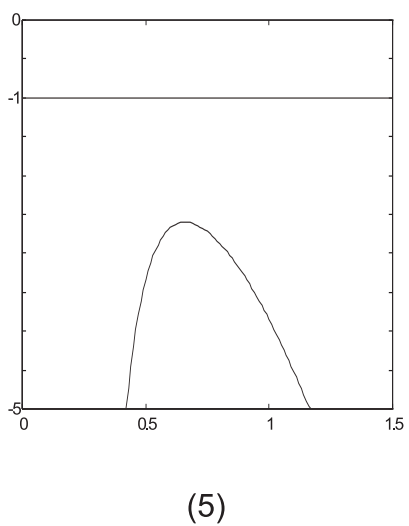
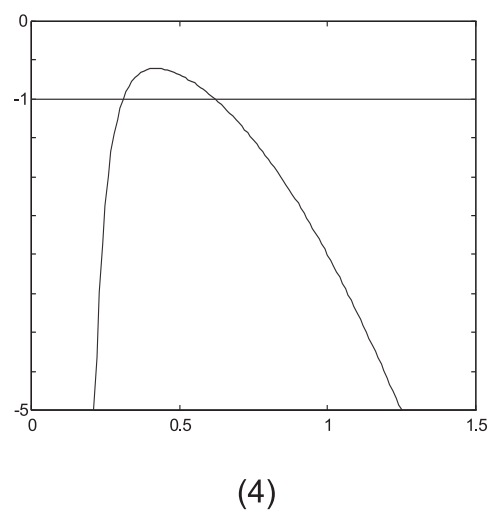
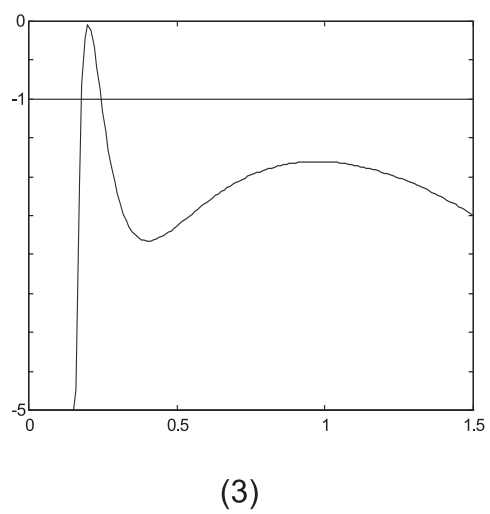
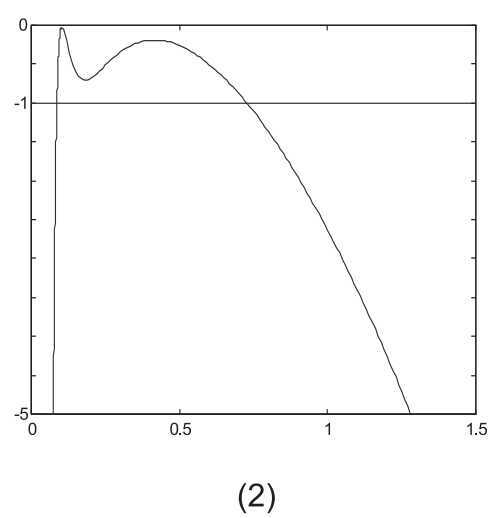
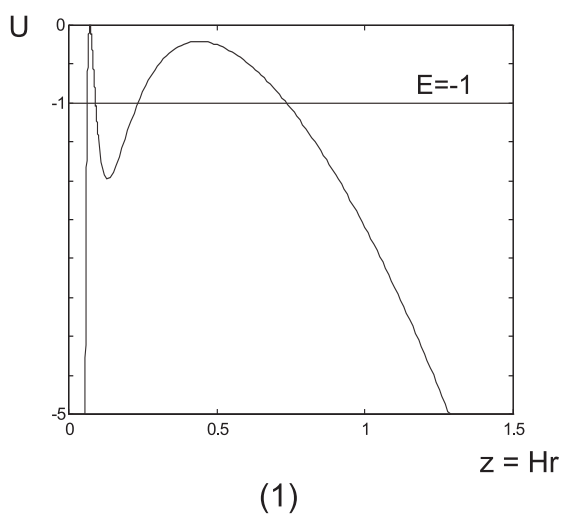


FIG. 3. Plots of the potential in each of the seven regions of Fig. 2. (1) ( $\tilde{\eta} = 0.5$ ,  $m = -0.07$ ), (2) ( $\tilde{\eta} = 0.5$ ,  $m = -0.1$ ), (3) ( $\tilde{\eta} = 1.5$ ,  $m = -0.2$ ), (4) ( $\tilde{\eta} = 0.5$ ,  $m = -0.4$ ), (5) ( $\tilde{\eta} = 0.5$ ,  $m = -1$ ), (6) ( $\tilde{\eta} = 0.5$ ,  $m = 0.2$ ), (7) ( $\tilde{\eta} = 1.5$ ,  $m = 0.2$ ). The potential in region (1) possesses oscillating, collapsing and expanding domains. In region (2), the potential has a well but oscillations are not allowed classically. In region (3), the right maximum of the potential does not contain the motion. In region (4) and (6), the potential has a single maximum separating collapsing and expanding domains. In region (5) and (7), the single maximum is accessible. The motion is monotonic.

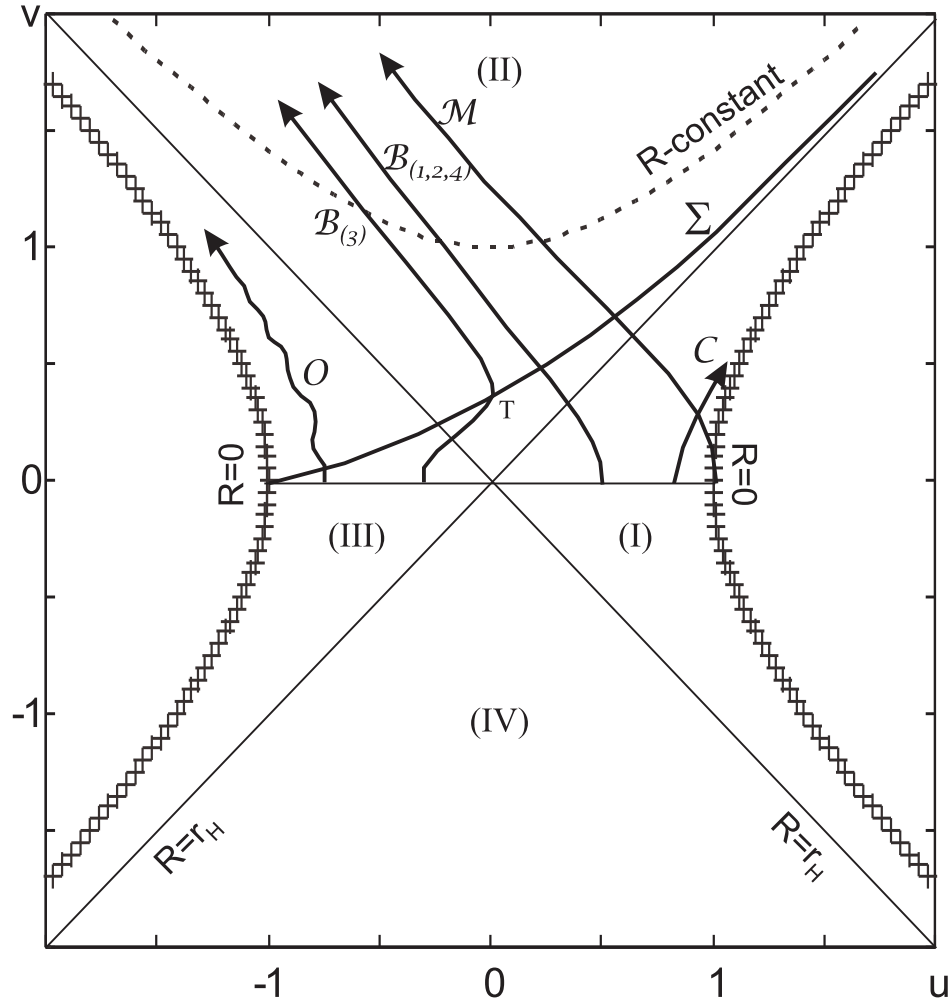


FIG. 4. Trace of the wall trajectories on a Kruskal-Szekeres diagram for  $\tilde{\eta} > 1$ . The physical exterior lies in region (II) and (III). An identical physically inaccessible copy is provided by the regions (I) and (IV). The oscillating trajectory,  $\mathcal{O}$  (region (1)) lies within the static region (III). The expanding bounce trajectory,  $\mathcal{B}_{(3)}$  also originates there but crosses the null surface  $u = -v$  to enter region (II), changing its angular direction at  $T$ . The trajectory lies completely inside the physical region. The collapsing trajectory  $\mathcal{C}$  lies within the unphysical region (I). The remaining bounces  $\mathcal{B}_{(1),(2),(4)}$  and the monotonically expanding  $\mathcal{M}$  trajectories originate in the unphysical region but cross the horizon to enter (II).

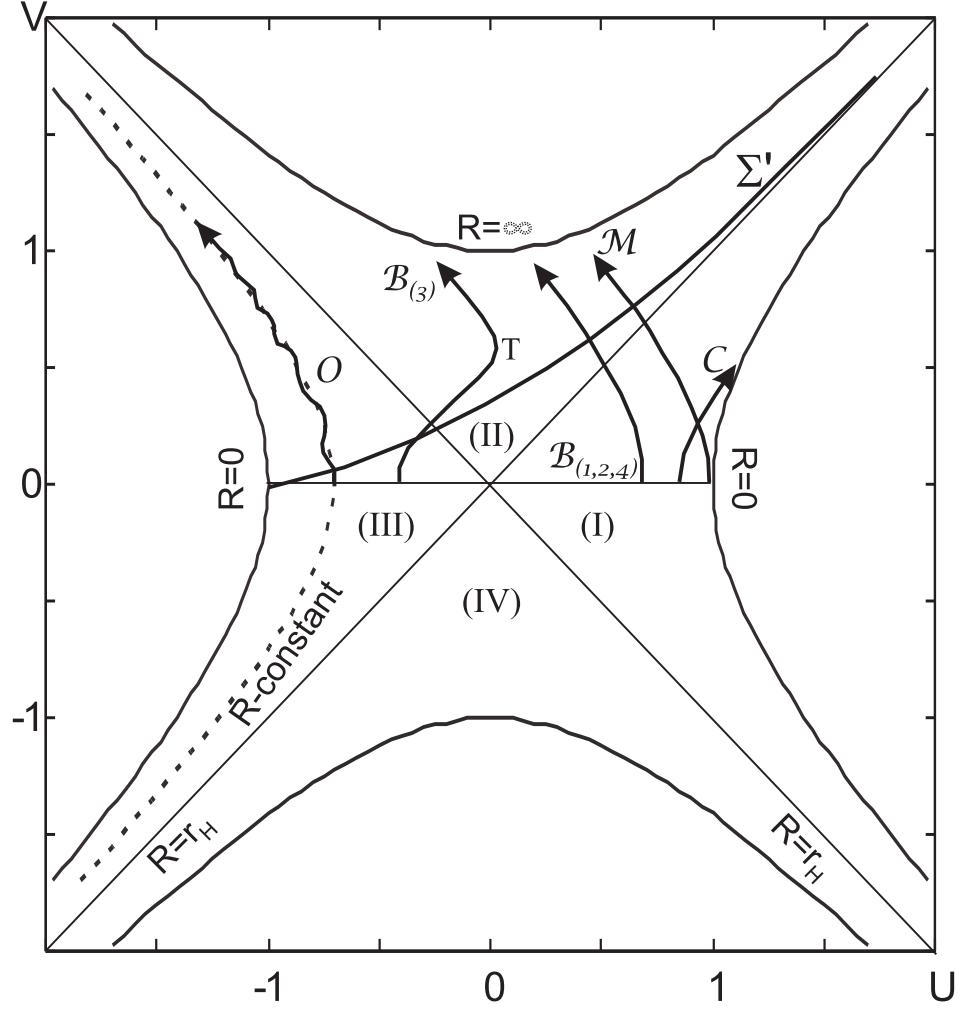


FIG. 5. Trace of the wall trajectories on a Gibbons-Hawking diagram for  $\tilde{\eta} < \sqrt{\lambda}$ . The oscillating trajectory,  $\mathcal{O}$ , lies completely within (III). The expanding trajectory,  $\mathcal{B}_{(3)}$ , lies completely within (II) and (III). It changes its angular direction within (II). The collapsing type  $\mathcal{C}$  trajectory, as well as both expanding  $\mathcal{B}_{(1),(2),(4)}$  and  $\mathcal{M}$  trajectories originate outside of the horizon.  $\mathcal{B}$  and  $\mathcal{M}$ , however, cross the horizon and enter (II).  $\mathcal{B}_{(1),(2),(3),(4)}$  and  $\mathcal{M}$  move asymptotically to the left.

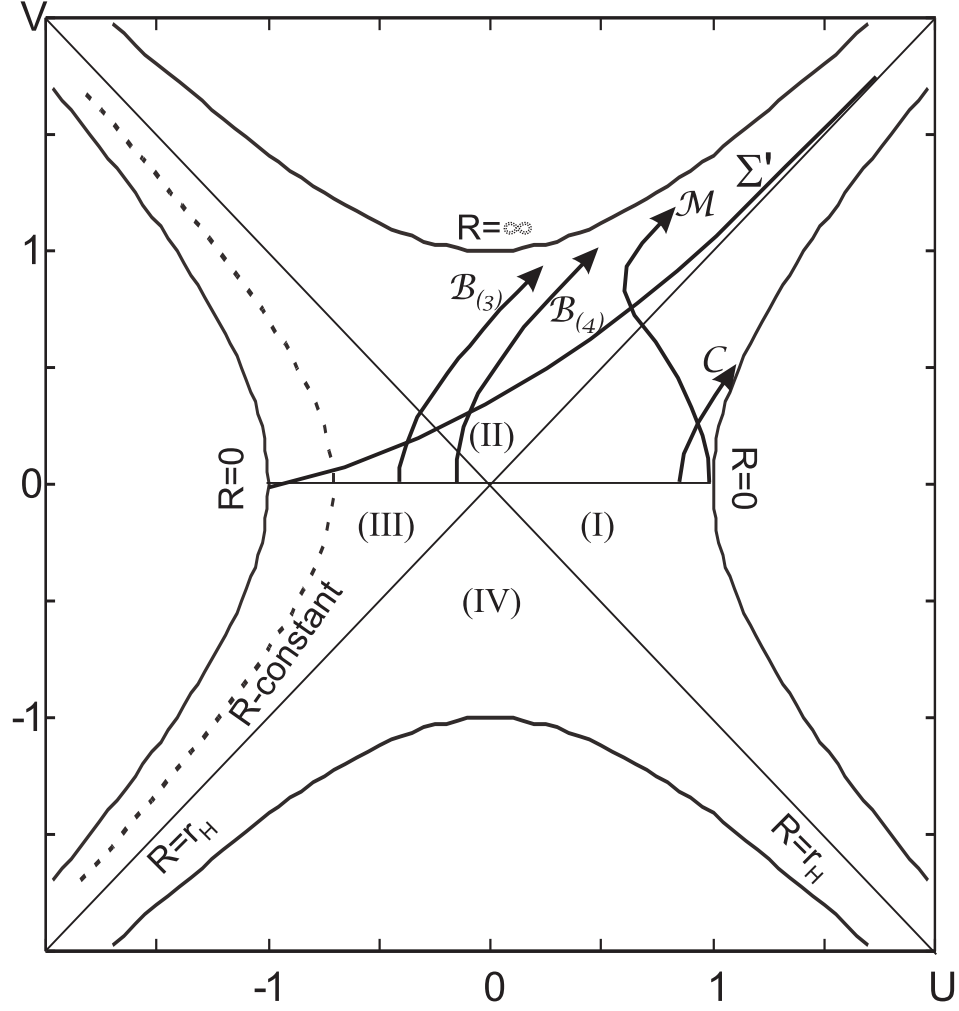
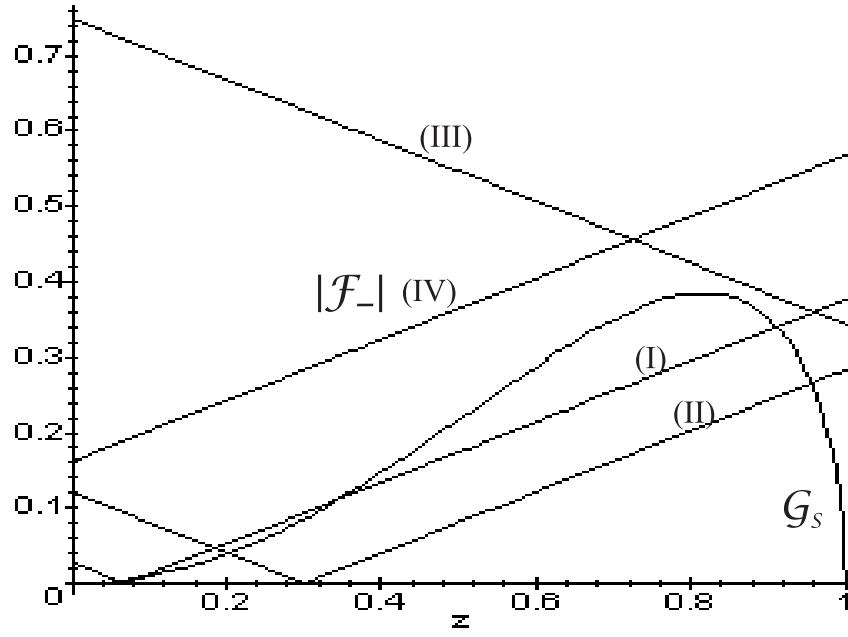
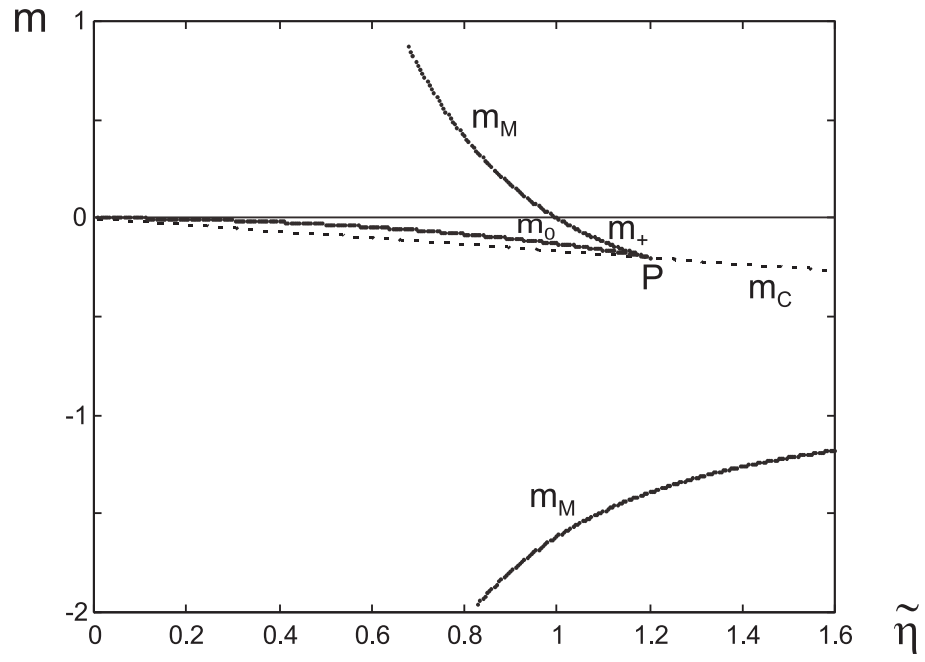


FIG. 6. Trace of the wall trajectories on a Gibbons-Hawking diagram for  $\tilde{\eta} > \sqrt{\tilde{\lambda}}$ . The expanding trajectories,  $\mathcal{B}_{(3)}$  and  $\mathcal{B}_{(4)}$ , lie completely within (II) and (III). The collapsing type  $\mathcal{C}$  trajectory as well as expanding  $\mathcal{M}$  trajectory originate outside of the horizon.  $\mathcal{M}$ , however, crosses the horizon and then changes its angular direction in (II).  $\mathcal{B}_{(3),(4)}$  and  $\mathcal{M}$  move asymptotically to the right.



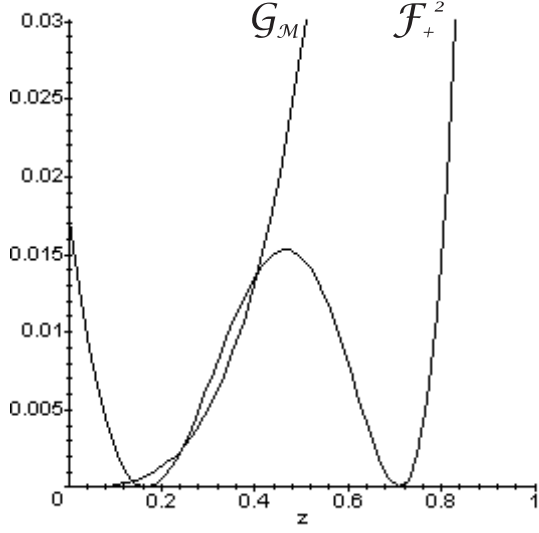
(a)



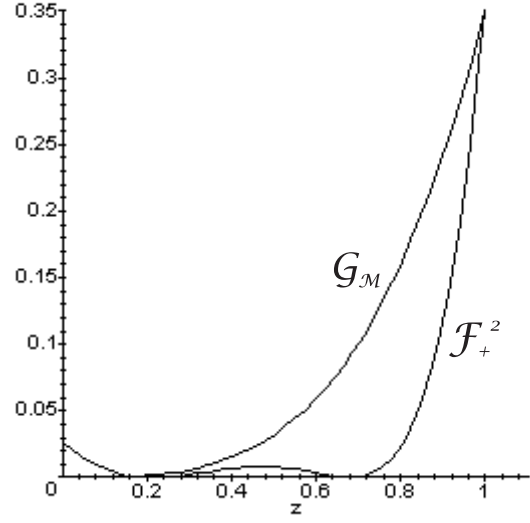
(b)

FIG. 7. (a) Plots of  $|\mathcal{F}_-|$  vs.  $z$  and  $\mathcal{G}_s$  vs.  $z$  with fixed  $\tilde{\eta} = 0.9$ . With a small negative mass (I:  $m = -0.07$ ), there are four intersections corresponding to bouncing points in the potential. As  $m$  decreases, oscillation disappears (II:  $m = -0.3$ ) and then the wall trajectory becomes monotonic (III:  $m = -1.85$ ) as in the case of positive mass (IV:  $m = 0.4$ ). (b) Parameter space with  $\tilde{\rho}_- = 0$  (Compare Fig. 2(a)) The only qualitative divergence from the generic behavior is that  $m_M$  diverges to  $-\infty$  as  $\tilde{\eta} \rightarrow 0$ .

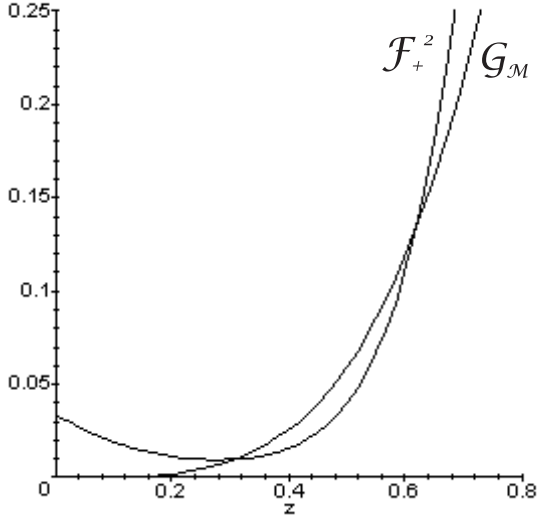




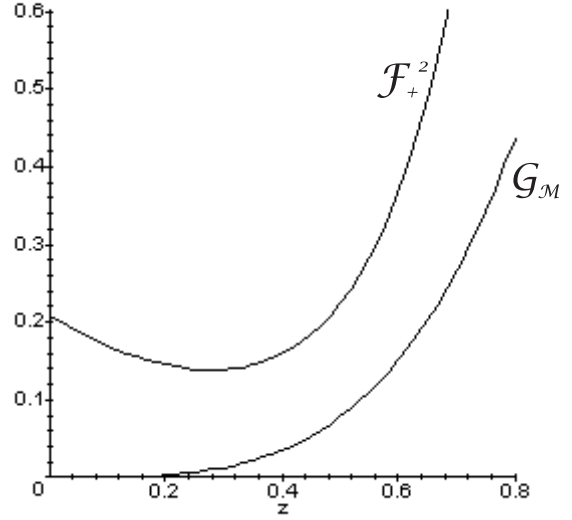
(a)



(b)



(c)



(d)

FIG. 8.  $\mathcal{F}_+^2$  vs.  $z$  and  $\mathcal{G}_M$  vs.  $z$  for  $\tilde{\eta} < 1$  in the four regions of parameter space: (1), (2), (4), and (5) (see Fig. 2). (a) region (1) ( $\tilde{\eta} = 0.9$ ,  $m = -0.16$ ), (b) (2) ( $\tilde{\eta} = 0.9$ ,  $m = -0.2$ ), (c) (4) ( $\tilde{\eta} = 0.5$ ,  $m = -0.4$ ), and (d) (5) ( $\tilde{\eta} = 0.5$ ,  $m = -1$ ).  $\mathcal{F}_+$  is positive in the central physical domain of  $\mathcal{F}_+^2$  in (a) and (b) while it is negative in the other two. Intersections of  $\mathcal{F}_+^2$  and  $\mathcal{G}_M$  indicate the turning points of the potential. In (a), the last intersection on the top right is not shown.

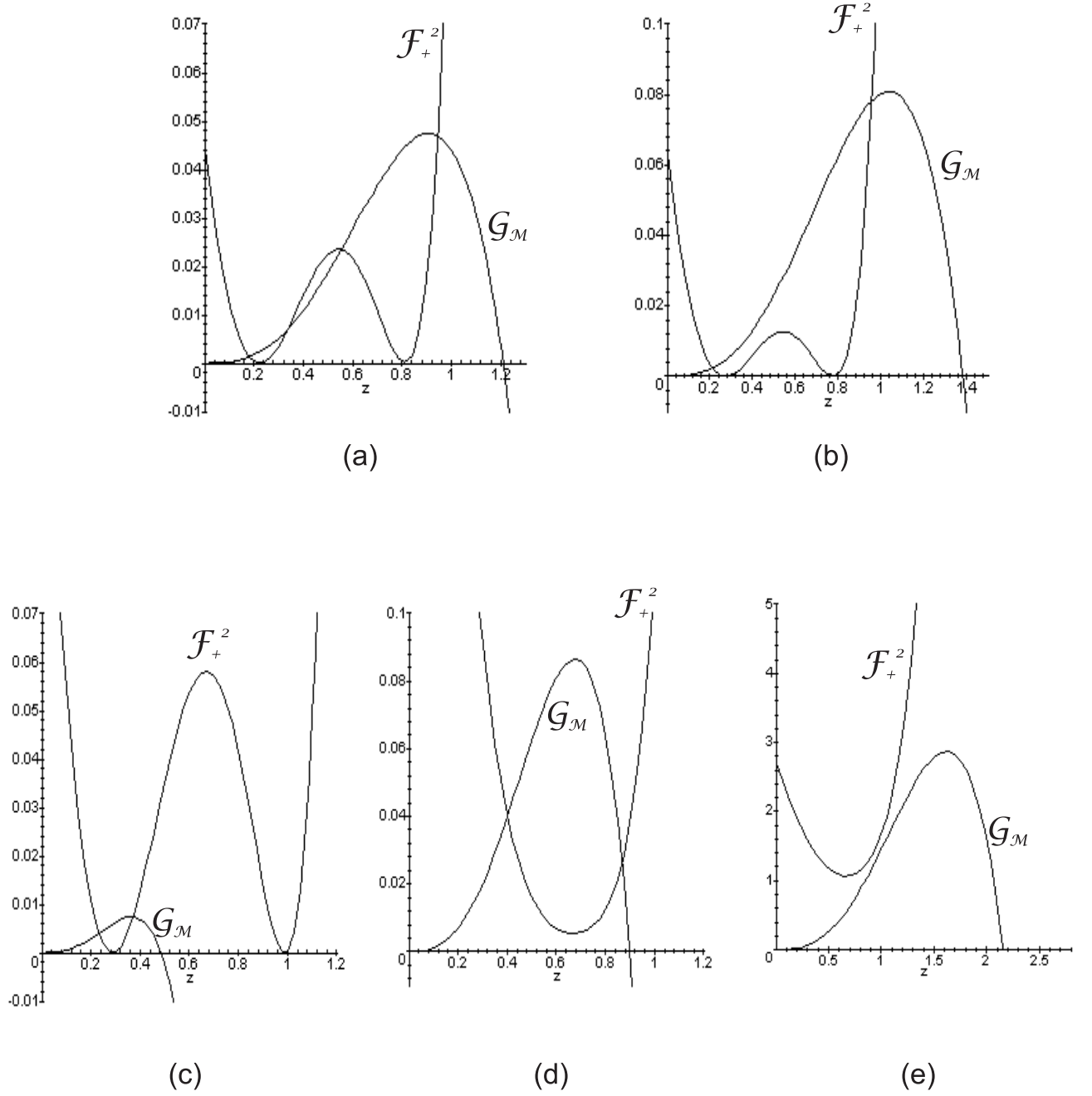


FIG. 9.  $\mathcal{F}_+^2$  and  $\mathcal{G}_M$  vs.  $z$  for  $\tilde{\eta} > 1$  in the five regions, (1) to (5) of Fig. 2: (a) region (1) ( $\tilde{\eta} = 1.1$ ,  $m = -0.21$ ), (b) (2) ( $\tilde{\eta} = 1.1$ ,  $m = -0.25$ ), (c) (3) ( $\tilde{\eta} = 1.5$ ,  $m = -0.27$ ), (d) (4) ( $\tilde{\eta} = 1.5$ ,  $m = -0.5$ ) and (e) (5) ( $\tilde{\eta} = 1.5$ ,  $m = -1.2$ ).  $\mathcal{F}_+$  changes sign on the expanding domain in (c).  $\mathcal{G}_M$  vanishes at  $z = 0$  and at the exterior horizon.

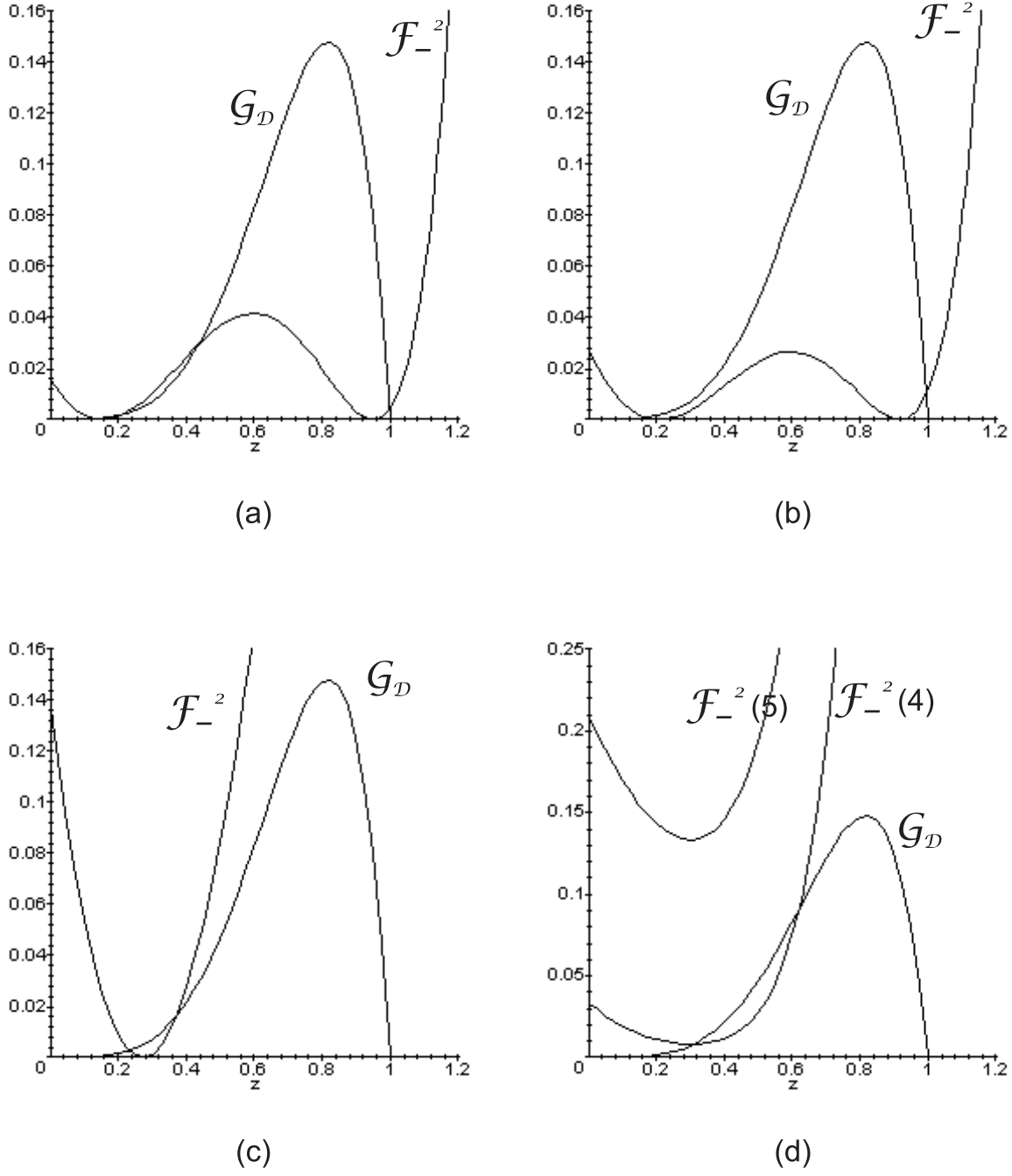


FIG. 10.  $\mathcal{F}_-^2$  and  $\mathcal{G}_D$  vs.  $z$  for  $\tilde{\eta} < \sqrt{\lambda}$ . (a) region (1) ( $\tilde{\eta} = 0.9$ ,  $m = -0.15$ ), (b) (2) ( $\tilde{\eta} = 0.9$ ,  $m = -0.2$ ), (c) (3) ( $\tilde{\eta} = 1.5$ ,  $m = -0.27$ ), (d-4) (4) ( $\tilde{\eta} = 0.5$ ,  $m = -0.4$ ) and (d-5) (5) ( $\tilde{\eta} = 0.5$ ,  $m = -1$ ).  $\mathcal{F}_-$  is positive on the central physical domain and negative in the others. In (c), the right part of  $\mathcal{F}_-^2$  is not shown.

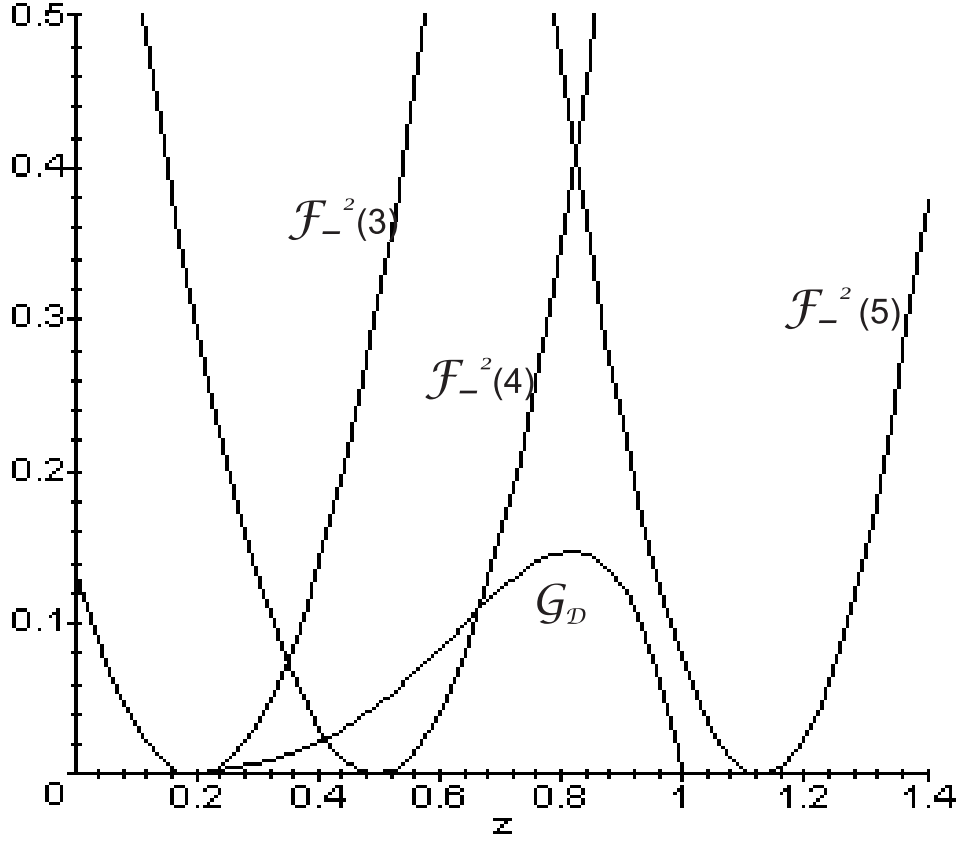


FIG. 11.  $\mathcal{F}_-^2$  and  $\mathcal{G}_D$  vs.  $z$  for  $\tilde{\eta} > \sqrt{\tilde{\lambda}}$  in region (3) ( $\tilde{\eta} = 2$ ,  $m = -0.2$ ), (4) ( $\tilde{\eta} = 2$ ,  $m = -0.5$ ) and (5) ( $\tilde{\eta} = 2$ ,  $m = -1.2$ ).  $\mathcal{F}_-$  is positive in the domain of increasing  $\mathcal{F}_-^2$ . In region (5),  $\mathcal{F}_-$  changes sign in the expanding domain.